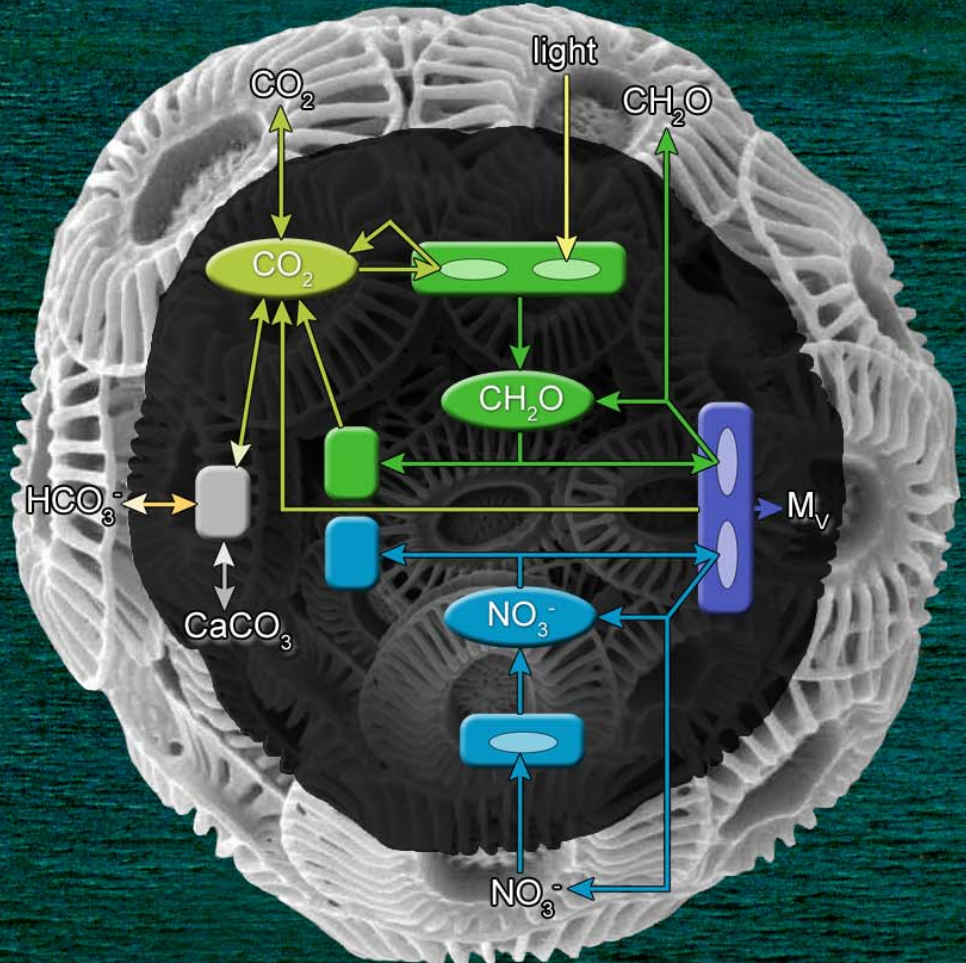


Modeling *Emiliana huxleyi*

photosynthesis, calcification, and the global CO₂ increase

Jorn Bruggeman



Modeling *Emiliana huxleyi*

photosynthesis, calcification, and the global CO₂ increase

Jorn Bruggeman

Supervision: C. Zonneveld
S.A.L.M. Kooijman

February 2000 – July 2001
Vrije Universiteit, The Netherlands

cover: the white cliffs of Dover are mainly composed of coccoliths



Table of contents

Introduction	5
Modeling theory: Dynamic Energy Budgets	7
The individual organism	7
The importance of size	8
Basic modeling units: elements and energy	8
Classification of organism content	9
Generic transformation kinetics	10
Food uptake	12
Reserve kinetics	13
Maintenance and growth	15
From individual to population	16
Model construction	18
About physiology	18
Use of the DEB framework	20
Model construction	20
Methods of analysis	26
Steady state analysis	26
Data fitting	28
Results and discussion: model I	30
Comparison with data	30
Model behavior	32
Quality of fit	33
Improving the model	34
What to change?	34
Implications for steady state analysis	37
Results and discussion: model II	39
Comparison with data	39
Model behavior	40
Discussion	41
Model test case: effects of a global CO₂ increase	42
Methods	42
Results	42
Discussion	44
General discussion	45

Summary 47

Literature 48

Appendix A: Equations and parameters of model I..... 50

Appendix B: Equations and parameters of model II 52

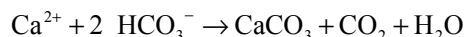
Appendix C: When to use fluxes instead of concentrations..... 54

Introduction

Interaction between the global climate and the world's biota is by no means a one-way street. Certainly, climate-related parameters like temperature and humidity play a major role in shaping the biological world. However, it has become more and more clear that biota in turn exert significant influences on our climate. In particular, they may affect the process of global warming.

Generally, global warming is attributed to human-induced increases in the concentration of greenhouse gasses, of which carbon dioxide is most renowned. Indeed, the increase in CO₂ has been shown to correlate well with the increase in human activities (e.g. the onset of the industrial revolution). However, full knowledge of human emissions will not suffice to predict future developments in the atmospheric CO₂ concentration on a quantitative level. Carbon dioxide is a key compound in the global carbon cycle. This cycle features several vast, predominantly biological sinks and sources of carbon (esp. photosynthesis and respiration), which are each either directly or indirectly linked to atmospheric CO₂. The cycle as a whole controls the availability of all carbon species, including carbon dioxide. A change in human emissions will undoubtedly affect carbon fixation and release of various sinks and sources, resulting in feedback loops of an as yet unknown nature. Clearly, one cannot reliably predict future atmospheric CO₂ concentrations without having charted every step in the carbon cycle.

A crucial part of the global carbon cycle is localized in the oceans. Not only do these harbor about 20 % of the earth's photosynthesis, they also constitute the sole site of calcite (CaCO₃) formation. The main part of marine photosynthesis is performed by unicellular algae, rather than more conspicuous macroscopic species. Likewise, the main part of marine CaCO₃ production has been suggested to be the work of a group of unicellular algae called coccolithophorids (rather than the work of corals, for instance). This ubiquitous group fixes CaCO₃ internally in wheel-shaped coccoliths, which are subsequently exported and incorporated in an external shell. Calcification (i.e. CaCO₃ fixation) occurs in the following reaction:



Coccoliths are relatively stable: when sinking to the ocean floor, only a small part of the CaCO₃ dissolves. Hence, sediments containing coccolithophorids often hold large amounts of CaCO₃ (e.g. the white cliffs of Dover). Like any other alga, coccolithophorids also perform photosynthesis: they consume CO₂ under influence of light, and use the carbon to synthesize numerous organic carbon-containing compounds. Note that calcification and photosynthesis are counteracting processes with respect to CO₂: the former produces it, while the latter consumes it. It is therefore doubtful where any CO₂ produced in calcification ever leaves the cell. At any rate, coccolithophorids affect the availability of several carbon species: at the very least, they remove bicarbonate, and produce both organic carbon and calcite. Combined with the fact that several coccolithophorid species are very common, the impact of this group on the global carbon cycle is likely to be substantial.

To obtain quantitative data about the current role of coccolithophorids in the carbon cycle, simple experiments might suffice. Carbon production and consumption rates, combined with a measure of abundance could provide an adequate picture. However, when one aims to predict developments in the global climate, experiments that focus on one particular (set of) species come up short: global changes depend fully on large-scale interactions between physical, chemical and biological processes. All these should be accounted for to arrive at a reliable prediction. This is far beyond the grasp of any experiment. Instead, one must resort to the use of models. Unlike experiments, they can describe the behavior of single species, and yet allow for application in a much broader context. Evidently, the goal of describing the role of coccolithophorids in the global carbon cycle is best served by the construction of a model.

Thus far, efforts to model any aspect of coccolithophorids have been extremely limited. Even most experiments have to date focused on the role of only one environment variable at a time (e.g. ambient light, CO₂ or nitrate), telling us little about more realistic, complicated scenarios of multiple nutrient limitation. This project aims to model the physiology of one the most common, and most studied coccolithophorids: *Emiliana huxleyi*. This species is found in all oceans, and can form extensive blooms during the summer. Primarily, we constructed the model to allow for application in climate-related research, in particular that dealing with the interaction between *Emiliana* and ambient carbon species. In addition, the model incorporates the availability of light and ambient nitrate, which is in keeping with recurrent experiments, and somewhat broadens the model's applicability.

The model is built on the framework provided by the Dynamic Energy Budget (DEB) theory (Kooijman, 2000). The DEB approach focuses on the properties of individual organisms, and generally results in mechanistic, dynamic models. DEB-based models explicitly obey the laws of mass- and energy conservation, which is obviously essential for any model that describes (part of) the geochemical element cycles.

This paper is built up as follows: first, I describe the key concepts of DEB theory. These are subsequently applied to render an initial *Emiliana* model. The behavior of this model is compared with the results of a characteristic coccolithophorid experiment, dealing with the effect of light limitation on carbon production rates. Results indicate some serious model shortcomings, and give cause for modification of the model. The model is revised, and again compared with light-limitation data, which now renders significantly improved results. Subsequently, I present an example of the application of the model in its targeted area of research: it is used to describe the effect of an increase in ambient CO₂ on organic- and inorganic carbon synthesis. The final chapter discusses various aspects of the model's quality and usability.

Modeling theory: Dynamic Energy Budgets

The Dynamic Energy Budget (DEB) theory aims to be a generic framework for modeling mass- and energy flows in biota. Clearly this is no trivial objective, for the underlying processes are neither restricted to one particular level of organization (e.g. cell, individual or population), nor to a particular species or group of species. In effect, DEB theory can build on none but the most basic organism characteristics.

In this chapter, I will describe the key concepts of the DEB theory. These include the following:

- Characteristics of the individual serve as the basis for all modeling decisions.
- Structural organism volume is the primary state variable in all DEB-based models.
- One or more additional state variables representing stored reserves can be added.
- Transformation kinetics (amongst others responsible for the merging of metabolic fluxes) are based on biochemical, balance-law-obeying concepts.
- Food uptake kinetics is identical to that of the most simple transformation, that with one substrate and one product.
- All food taken up is initially transferred to the reserves.
- Reserves supply nutrients and energy to maintenance, growth and reproduction.
- A population of individuals can be described as one single individual for which its surface area is proportional to its volume.

While the following presents an adequate summary of a number of key concepts of DEB theory (though by no means all concepts), at some points, argumentation might differ from that given by Kooijman. For a full overview of DEB theory, I refer to the book ‘Dynamic energy and mass budgets in biological systems’ (2nd edition, Kooijman, 2000).

The individual organism

The DEB theory was designed to provide a modeling approach that is not restricted to one particular level of biological organization. It should be applicable to processes at a biochemical scale as well as to those at a global scale, while maintaining the same core of assumptions and concepts.

Clearly, the most straightforward way of integrating multiple levels of organization is to create a basic model of the lowest relevant unit in the hierarchy, and link multiple of such models to work the way up to higher levels. For instance, one could imagine a generic model for biochemical transformations, which serves as the basis for a model of a single cell, an organ, an organism, a population, an ecosystem, just by repeatedly chaining low-level models. For such a modeling approach to work, however, two conditions must be met: first, the biological unit that is chosen as the basis for all others must function as a whole, independent of specific interactions that occur at the level of subunits. Second, the model must include the properties that are responsible for the formation and coherence of higher-level units. To illustrate the second condition: a modeling approach that focuses on behavior might link the individual and population levels of organization, but it is unlikely to have any relevance at the biochemical level. Thus it would fail the goal of being applicable at every level or organization.

In most biological research, the very rock bottom level of biological organization is placed at the level of biochemistry. This would favor a modeling approach that takes biochemical processes as its main low-level unit. However, such an approach is not feasible. To start with, it requires knowledge of every biochemical process that occurs in the species one desires to study. This knowledge is currently not available, and will probably not become available for a very long time. Secondly, the vast complexity that would result from a biochemical modeling approach, in particular when dealing with

complete organisms or ecosystems, would make all forms of model analysis impossible, if only because the lack of computing power. Hence, we need to step away from biochemistry as the basic level, and resort to a higher unit of organization that still conforms to the requirement of (relative) autonomy.

In this case, a natural starting level is that of the individual organism. An individual-based approach strongly reduces complexity when compared to a biochemistry-based one, and thus allows for application at the level of populations and ecosystems. Also, the individual is the lowest level of biological organization that functions independently as a living unit. Thus it can be, and has been studied with relative ease, resulting in an ample supply of information that can assist at the modeling of individual-specific processes. Note that, even though the DEB framework focuses on the individual as a whole, this by no means implies that specifics of biochemistry cannot be included (for instance, the *Emiliana* model described in this paper contains biochemical pathways). It merely promotes the viewing of biological phenomena like feeding, reproduction and production of substances as being specific to individual organisms as a whole, rather than being a function of their biochemical characteristics.

The importance of size

The choice to use the individual as the basis of the DEB framework has many consequences; in effect it specifies that properties of individuals as a whole should stand at the basis of all further modeling choices. In particular, this has consequences for the choice of state variables.

State variables describe the state of a model. In a given environment (with known values for the input variables) the exact behavior of the model is defined by the value of its state variables. If state variables are absent, the model is static: it always responds the same to given circumstances. Clearly, this would not be fit for a mass- and energy focused model of individual organisms: during different moments in its life, an individual could respond very different to one particular set of circumstances. Aspects like food uptake, energy requirement, and reproduction are all likely to depend on the state of the individual. Hence, a realistic framework for the modeling of individuals should include at least one state variable.

One characteristic of individuals that clearly qualifies as a part of their state is size. Large individuals eat more than small ones, they require more energy, they are more likely to reproduce. A measure of size will thus be indispensable in predicting the behavior of an individual. However, choosing one universally applicable size state variable from the numerous measures of size that exist is not easy. Characteristics like mass, volume and surface area may each control a particular set of size-related aspects: whereas an individual's volume or mass is likely to determine characteristics like energy requirement and metabolic rates, its surface area is likely to control interaction with the environment, e.g. heat dissipation and unicellular food uptake. Neither measure of size can be missed. Fortunately, these different manifestations of size are not independent of each other. For instance, most species roughly maintain their shape during growth, which implies that their surface area will be proportional to their volume to the power $^{2/3}$. Thus, when the volume of an organism is known, its surface area will be easy to determine, and vice versa.

To allow for a strong influence of both volume and surface area, the individual's size is represented in the DEB framework by its volume; any surface area specific properties are simply taken proportional to volume $^{2/3}$.

Basic modeling units: elements and energy

Any model aiming to describe quantitative aspects of nutrient handling will need to monitor all input, output and incorporation of substances. Key players in this field are the laws of mass and energy

conservation: an inflow must result in outflow or addition to the individual. Quantitative models that fail to obey those laws are hard to take seriously.

Conservation laws can be implemented in various ways. For instance, mass balances can be maintained at levels ranging from protons to macromolecules. Since the main requirement for a mass balance unit is indestructibility, DEB theory focuses on chemical elements: the highest chemical unit that is not modified by biological processes. Accordingly, every substance taken up or exuded has to be defined by its ratio of chemical elements. For simplicity most DEB applications only check C, H, O and N balances, but the number of elements monitored is not restricted in principle by DEB theory. Extension of balances to include energy is straightforward: for every substance its chemical potential should be defined. Not in every DEB model both balances should be maintained; depending on one's interests, either (but not both) could be excluded. The model dealt with in this paper focuses on mass balances only. For this reason I will describe only the mass-related aspects of DEB theory.

Classification of organism content

The core of an organism's nutrient handling in terms of elements and energy lies at the chemical level. When individual-based processes like hunting and feeding are complete, the nutrients enter the network of metabolic pathways that in the end determines the fate of every atom consumed. Undoubtedly, the most true-to-life nutrient-monitoring approach would include each and every step in these pathways, thus providing complete predictions for the production rate and concentration of every substance involved. However, this would require one state variable for every compound: a goal not attainable and not worth pursuing, as it would result in a setup far too complex to analyze. Also, when we take a closer look to chemical content of organisms, such complexity seems rather superfluous: the ratio at which most compounds are present is near constant, which implies that a known concentration of just one compound suffices to predict the concentration of most others. This allows for a very straightforward manner of simplification: to describe an organism's content, we can suffice by creating one state variable for every group of compounds that tend to show up in a constant ratio. Providing the ratio between the lumped compounds is in reality near constant, the model's description of reality does not suffer.

For the categorization and combining of compounds, DEB theory makes use of the fact that most vital constituents of every organism are present in a near constant ratio. Based on this observation, DEB theory assumes 'strong homeostasis', i.e. the vital part of every organism is of a constant composition. This generalized vital component is referred to as the structural part of an organism. In practice, the list of compounds that obey 'strong homeostasis' and consequently can be categorized as structure comprises almost all organism constituents. Thus, 'structure' becomes a collective for an extremely diverse set of compounds, ranging from DNA and proteins to lipid membranes and cell walls.

Although one could assume the entire individual to consist of structure (i.e. to have a constant composition), in some situations this fails to describe important behavior. A phenomenon for which the use of structure alone is insufficient is buffering of food. Most organisms live in environments with fluctuating food density. They are able to endure periods of food scarcity, but only if these are preceded by periods of abundance. This suggests that they are able to buffer the food taken up, enabling them to fulfill their energy requirement at all times. Numerous examples of food buffering are known, ranging from nitrate storage in the vacuole of unicellular algae to lipid storage in human fat cells. Food buffers are often directed to buffer a specific nutrient, which implies that their composition can differ radically from that of the organism as a whole. Because of this difference in composition, the decrease of a specific buffer during food scarcity can cause extensive changes in average organism composition. This particularly contrasts with the behavior of a structure-only model.

DEB theory has been constructed to deal with food buffering specifically. Next to structure, it allows for the existence of reserves: state variables that represent the buffered assimilated substances. Like structure, reserves are generalized compounds of a constant composition. Consequently, two or more reserve substances can be combined into one single reserve variable only if they are present in a constant ratio. If their ratio varies significantly, their average composition will not be constant, thus requiring separation into multiple reserves. Yet there is no need to aim for a complete classification of every single compound whose concentration varies independently of structure or other reserves. Two main reasons exist for including a reserve in a DEB-based model: (1) in reality, the average organism composition fluctuates through significant increases and decreases of the reserve independent of structure and other reserves, and (2), temporary food scarcity does not necessarily result in death, because required energy and nutrients appear to be buffered.

Based on the categorization of organism content, we can now refine our approach to organism size described previously. Size should be included as a state variable because it controls various aspects of an individual's behavior. When dealing with mass- and energy balances, one can think of aspects like the (maximum) rate of food uptake, energy requirements, reproduction, the (maximum) growth rate, etc. Since some of these appear to be volume-related while others correlate with surface area, one of these measures of size, combined with a linking function to the other, will be an essential model component. Consequently the DEB-framework includes volume as state variable.

However, an individual's actual volume includes both structural- and reserve volume. If total volume were used to determine an organism's predominantly active characteristics like food uptake etc., the mere volume of the predominantly passive reserves would provide a rather undeserved boost in activity. Who would believe stored fat to significantly boost an individual's energy requirement or hunting rate? For as far as reserves do exert an influence (e.g. increased transportation costs, increased insulation), their effect is strongly dependent on the specific species and reserve compounds one is dealing with, which makes inclusion in the generic DEB framework impossible. Instead, partly because organism size is mostly used in an active context, partly because it results in simpler kinetics, the DEB framework focuses on structural volume: only the volume occupied by structural compounds matters for size-related behavior.

Structural volume is the primary state variable in the DEB framework. Most other (structural) measures of size can easily be derived from the structural volume. A link to the surface area is provided by the shape function (for isomorphs: $A \propto V^{2/3}$). The constant composition of structure (including its water fraction) implies a clean, proportional relationship with both structural mass and weight.

Whereas structure is measured in volume, all reserves are specified in densities: reserves mass (or energy) per structural volume. This facilitates a biochemically oriented approach, in which a compound's concentration determines reaction rates rather than its absolute mass, weight or volume.

Summarizing, the DEB framework includes the following state variables:

structural volume V , dimension $length^3$

reserve densities $[M_E]$, with E being the reserve identifier, dimension $mass \cdot length^{-3}$

This applies only when dealing with mass balances. If energy balances are checked, reserves are specified as $[E]$, with dimension $energy \cdot length^{-3}$.

Generic transformation kinetics

As in any model that deals with mass- and energy balances of organisms, substance transformations play an essential part in the DEB framework. Consumed food needs to be transformed into reserves, assimilated products need to be transformed into structure. This can involve simple one-substrate transformations, converting a substance into one or more products, but also more complicated ones.

The nature of the modeled transformations will depend strongly on the number and nature of food- and reserve types involved: as one distinguishes more food types to target one reserve (as non-interchangeable substrates), reserve synthesis will become more complex; as one distinguishes more substrates (i.e. reserves, as will be shown later) to target structure-synthesis, the combining, structure-producing transformation will become more complex. For instance, whereas ‘lion structure’ may be produced from one generalized ‘prey-compound’, ‘plant structure’ is likely to be produced from separate nitrogen-containing (NO₃⁻, NH₄⁺) and carbon-containing (CO₂) compounds. Because transformation specifics are strictly dependent on the targeted species, the DEB framework merely supplies generic transformation kinetics, which can deal with any number of substrates.

All significant transformations occurring in organisms are enzyme-mediated. This should be reflected in the transformation kinetics one applies: it has to be enzyme-based. Particularly it should involve some kind of saturation: when substrate is abundant, the transformation rate should draw near a maximum. A number of approaches for multiple substrate kinetics exist, but a combination of a good foundation and simplicity is rare. While the single-limiting-nutrient approach of Droop gives results that are highly realistic, it lacks a mechanistic explanation. Also it presents problems in situations where multiple substrates are simultaneously limiting (Zonneveld, 1995). On the other hand classic enzyme kinetics (pseudo steady state, concentration-based) is well founded and accepted. However, extending it to large numbers of substrates is complicated. The kinetics cannot always be found analytically, and even if an analytic solution is available, the vast number of parameters make inclusion in the model less than tempting.

Because transformations play such an important role in many DEB-based models, Kooijman tried to develop a mechanism that is both simple and mechanistically sound. Departing from classic concentration-based pseudo-steady state kinetics, he arrived at the so-called Synthesizing Unit (SU). This represents an enzyme that binds substrate irreversibly, i.e. substrate-enzyme dissociation rates are zero. An analytic solution for Synthesizing Unit kinetics is available for any number of substrates, and contains less parameters than full pseudo-steady state kinetics. For a one-substrate transformation, SU kinetics equals standard Michaelis-Menten. For a two-substrate transformation – which is the most complicated case dealt with in this paper – SU kinetics is given by the following formula:

$$J_{P,A} = \frac{1}{\frac{1}{J_{m,P}} + \left(\frac{\rho_{S_1,P}}{y_{S_1,P}} \cdot J_{S_1} \right)^{-1} + \left(\frac{\rho_{S_2,P}}{y_{S_2,P}} \cdot J_{S_2} \right)^{-1} - \left(\frac{\rho_{S_1,P}}{y_{S_1,P}} \cdot J_{S_1} + \frac{\rho_{S_2,P}}{y_{S_2,P}} \cdot J_{S_2} \right)^{-1}}$$

$J_{P,A}$	rate of product P synthesis (assimilation)
$J_{m,P}$	maximum rate of product P synthesis
$\rho_{S_i,P}$	binding probability of substrate S_i to SU producing P ($0 < \rho_{S_i,P} \leq 1$)
$y_{S_i,P}$	yield: units of substrate S_i needed for one unit of product P
J_{S_i}	rate of substrate S_i arrival

One of the most striking aspects of SU kinetics is that it deals with substrate fluxes instead of concentrations. In this SU kinetics deviates from its classic-enzyme-kinetics origin. The difference is only superficial, however. SU kinetics can easily be transformed into concentration-based kinetics by writing $k_{S_i} \cdot C_{S_i}$ (affinity constant multiplied by concentration) instead of $\rho_{S_i,P} \cdot J_{S_i} / y_{S_i,P}$. Note that in that case the yield constant $y_{S_i,P}$ will still be needed to determine the rate of substrate disappearance, i.e. the use of fluxes does not change the number of parameters.

The main benefit of the use of fluxes then lies not in effective differences with concentrations, but rather in the implicit simplification fluxes provide. Concentration-based transformation kinetics requires the substrate concentration at the reaction site to be known. For biological transformations

this would entail describing the substrate concentration inside the organism, which is possible only by including internal substrate concentration as a state variable. Also the compartmentalization of the organism often requires the substrate to pass one or more compartments before arriving at the reaction site. In that case the final substrate concentration is determined by the concentration in intermediate compartments, thus requiring the incorporation of yet more state variables. Since addition of state variables significantly complicates the model, it is clear that simplification of the above situation is desired.

Here flux-based kinetics shows its merit. Flux-based transformation rates are specified by substrate arrival rate. This approach can effectively skip any intermediate compartments, requiring no more than the last substrate arrival rate known before the transformation. Implicitly a number of assumptions are made, most importantly that in all intermediate compartments the substrate concentration is constant. Appendix C deals with the application of fluxes, and under what circumstances they can be a good approach.

Food uptake

After choosing the state variables for the model, one must define their in- and output fluxes. Because DEB models obey mass balance laws, all model compounds should be traceable to their import from the environment. This then is a natural starting point for defining substance fluxes.

By far, the most influx of substances occurs through feeding. Feeding processes are diverse, however, ranging from hunting of prey to uptake of molecules over the cell membrane. DEB theory aims to be a modeling framework for all organisms, and therefore requires a generic description of feeding rate. Kooijman has chosen to use standard hyperbole kinetics for this purpose. The uptake rate for food type X then becomes:

$$J_{X,A} = J_{m,X} \cdot \frac{X}{X + X_{\frac{1}{2}}}$$

As food density X increases, $J_{X,A}$ approaches the maximum rate of food uptake $J_{m,X}$. When X equals $X_{\frac{1}{2}}$, $J_{X,A}$ is half of $J_{m,X}$. The benefit of hyperbole kinetics is that it is already used in the description of highly diverse feeding behavior: the hyperbolic ‘functional response’ is the standard in ecology, while the mathematically identical Michaelis-Menten kinetics describes enzyme-mediated reactions like transport of substrates over the cell membrane.

As you may recall, one of the reasons for including a state variable representing size was that size influences characteristics like food uptake. DEB theory accounts for this by making the maximum rate of food uptake ($J_{m,X}$) proportional to the organism’s surface area. For single-cell organisms that take up nutrients over the cell membrane (as in this case) this is often assumed.

Because DEB theory was primarily developed for isomorphic organisms, it takes surface area to be proportional to volume^{2/3}. Then the maximum rate of food uptake also is proportional to volume^{2/3}, making it possible to define it as follows: $J_{m,X} = \{j_{m,X}\} \cdot V^{2/3}$. Here $\{j_{m,X}\}$ represents the surface-area-specific maximum rate of food uptake. It is important to note that V is used here in DEB context, i.e. it refers to structural volume rather than total volume. This implies that $V^{2/3}$ is no longer a true measure of surface area: it neglects volume occupied by reserves.

In part, this measure of surface area is used for the sake of simplicity. V already is a part of DEB models: it is the central state variable. If the actual volume were used to calculate the surface area, it would require evaluation of the reserve densities at numerous points in the model. This would result in implicit descriptions of feeding rate because of circular references (feeding, reserve turnover and growth would become more intertwined). In addition, it is likely that $J_{m,X}$ correlates better with the structural rather than the actual surface area in numerous situations. It all depends on the question: do stored reserves contribute to a higher feeding rate? Take a single-cell organism in which nutrients are

taken up by membrane-bound transporters. In that case one can hardly imagine a temporary increase of internal reserve volume (e.g. expansion of a nitrate vacuole) to produce more transporters. In this case nutrient uptake should be independent of reserve volume.

Reserve kinetics

In a default DEB model consumed food is first transferred to a reserve buffer. Assimilated substances then will have to pass the reserves before contributing to growth or maintenance processes. This construction may seem rather counter-intuitive. Most will assume assimilated food to be available for growth right away. Any reserve buffers could be located aside of the pool of assimilated food, and release their contents when that pool decreased in size (i.e. during food scarcity). A model implementing that construction, however, would require one or more additional state variables representing assimilated food. To prevent this complication, DEB theory assumes substance transfer between the ‘assimilated food’ pool and the reserves to be infinitely fast, compared to the rate at which assimilated food is used in catabolic processes. When this is assumed, the model’s behavior is indistinguishable from that of a model in which all food is first directed to reserves.

Generally reserve composition differs from food composition. If food assimilation flux $J_{X,A}$ is to be directed to the reserve pool, the model must include a food→reserve conversion in order to arrive at reserve assimilation rate $J_{E,A}$. DEB theory does not restrict food→reserve transformation types. I will give two examples of possible transformations. If one food type produces one or more different reserve types, one can define yield constants converting food into reserves: $y_{X,E}$ units of food X produce 1 unit of reserve E . If multiple food types are combined to produce one reserve type, $J_{E,A}$ can be based on synthesizing unit kinetics, with $J_{X,A}$ for substrate arrival rate.

Since all food is first directed to reserves, the latter are the sole substrate source for processes like maintenance and growth. Consequently reserves need to become available if growth and maintenance processes are to receive substrate. For this purpose DEB models include the catabolic flux $J_{E,C}$. When we combine the catabolic flux with the reserve assimilation rate, we can define the differential equation for reserve amounts (M_E):

$$\frac{d}{dt}M_E = J_{E,A} - J_{E,C}$$

From this the differential equation for reserve densities ($[M_E] = M_E/V$) can be derived:

$$\frac{d}{dt}[M_E] = [J_{E,A}] - [J_{E,C}] - [M_E] \cdot \frac{1}{V} \cdot \frac{d}{dt}V$$

Note that the $[M_E] \cdot V^{-1} \cdot dV/dt$ expression is a consequence of standard quotient (M_E/V) differentiation.

What is the value of the structural-volume-specific catabolic flux $[J_{E,C}]$? This is determined by three restrictions imposed on the reserve dynamics:

1. Reserve density at steady state should be independent of organism size (i.e. structural volume V) under fixed external circumstances. Kooijman calls this the weak homeostasis assumption.
2. Reserve availability (outflow) should not depend directly on food uptake.
3. Every reserve should be partitionable: when a multiple reserve compounds are present in a fixed ratio, and they contribute to maintenance and growth in the same ratio, it should be possible to combine them in one generalized reserve. This implies that an arbitrary part κ_A of any reserve

density should, when separated, produce κ_A of the original catabolic flux if its growth and maintenance contribution are κ_A of the original.

Combined these restrictions severely limit the possible kinetics of $[J_{E,C}]$:

- For reserve density at steady state ($d[M_E]/dt = 0$) to be independent of V , its differential should be proportional to V^x . Here the factor x can be any number, including 0. Commonly reserve assimilation $[J_{E,A}]$ is proportional to food uptake. This applies for instance if food type X is the sole source of reserve type E . Indirectly $[J_{E,A}]$ then is proportional to $V^{-1/2}$, as can be seen in the following formula:

$$[J_{X,A}] = \frac{J_{X,A}}{V} = \frac{\{J_{m,X}\} \cdot V^{2/3} \cdot f}{V} = V^{-1/3} \cdot \{J_{m,X}\} \cdot f \left(f = \frac{X}{X + X_{1/2}} \right)$$

Because restriction 2 dictates that $[J_{E,A}]$ cannot be part of $[J_{E,C}]$, weak homeostasis is possible only if the combined non-assimilative fluxes are proportional to $V^{-1/3}$. This then applies to the combination of structural-volume-specific catabolic flux and dilution by growth. In formula it translates to:

$$[J_{E,C}] + [M_E] \cdot \frac{1}{V} \cdot \frac{d}{dt} V = H(\dots) \cdot V^{-1/3}$$

for a function $H(\dots)$ that is independent of V .

- It can be proven that for reserve partitioning to be possible, the total reserve density outflow should be directly proportional to $[M_E]$. Combined with the above this corresponds to:

$$[J_{E,C}] + [M_E] \cdot \frac{1}{V} \cdot \frac{d}{dt} V = \dot{v}_E \cdot [M_E] \cdot V^{-1/3}$$

for some constant \dot{v}_E , which is independent of both V and $[M_E]$.

- Additionally reserve partitioning requires the proportion of the catabolic flux used for maintenance and growth combined to be independent of $[M_E]$.

Thus, the weak homeostasis and partitionability requirement lead to the following reserve dynamics:

$$\frac{d}{dt} [M_E] = [J_{E,A}] - \dot{v}_E \cdot [M_E] \cdot V^{-1/3}$$

The catabolic flux then becomes:

$$J_{E,C} = V \cdot [M_E] \cdot \left(\dot{v}_E \cdot V^{-1/3} - \frac{1}{V} \cdot \frac{d}{dt} V \right)$$

In a multiple-reserve model, this kinetics applies to every individual reserve pool, each with an individual \dot{v}_E . However, when multiple reserves function as non-interchangeable substrates for structure synthesis (e.g. separate C-containing and N-containing reserves in plants), the differential for reserve densities changes slightly. In that case the lack of one particular reserve can prevent structure synthesis, thereby decreasing utilization of the catabolic fluxes of other reserves. DEB theory defines

part of those ‘rejected reserves’ to return to the reserve pool, i.e. when one nutrient is lacking, others can – to some extent – dam up in reserves. Hence the reserve pool receives additional input (or, if you like, its outflow is decreased), represented by $\kappa_E \cdot [J_{E,R}]$:

$$\frac{d}{dt}[M_E] = [J_{E,A}] - \dot{v}_E \cdot [M_E] \cdot V^{-1/2} + \kappa_E \cdot [J_{E,R}]$$

Details about this reserve-return can be found in next paragraph.

Maintenance and growth

Most DEB models include three destinations for the catabolic flux $J_{E,C}$: reproduction, maintenance and growth. Reserves allocated to reproduction are buffered and, at some moment in time, transformed into offspring. Because the *Emiliana* model described in this paper does not monitor individual reproduction, it does not implement the reproduction sink. Therefore I will not discuss this aspect any further.

Structural matter combines a set of (bio)chemically extremely diverse compounds. As the ratio of these compounds is assumed constant, individual rates of synthesis and destruction will be strictly synchronized: structure grows and diminishes as a whole. When viewed from a distance, this indeed seems to apply to most organisms. However, any biologist will realize that an organism whose size appear to be static, still perform synthesis of most of its structural compounds. All its constituents are subject to deterioration, and the appearance of a constant composition is maintained only by continuous resynthesis. This applies to chemical compounds like proteins and mRNA’s, but also to high-level units like red blood cells. Since such ‘maintenance’ of structure is likely to require significant quantities of nutrients or nutrient derivatives, it needs to be incorporated in the DEB framework.

Obviously, maintenance cannot be implemented as continuous destruction and resynthesis of structure as a whole, for that would imply that all structural compounds deteriorate at the same rate. Hence, the DEB framework defines structure to require a fixed amount of substances (or energy, if one chooses to check energy balances) per time. This amount is assumed proportional to structural volume: $J_{E,M} = [J_{E,M}] \cdot V$; no reserve maintenance is included. $J_{E,M}$ is subtracted from the catabolic flux, and is usually defined for every reserve type individually. Thus, the average composition (e.g. element ratio) of matter invested in maintenance can differ radically from that required for growth. Differences in turnover rate between individual structural compounds can therefore be accounted for. In most implementations of the DEB framework, maintenance is considered essential for survival of the organism; when the supply of available nutrients drops below the level required for maintenance, the individual dies.

When maintenance costs have been paid, the remainders of the catabolic flux become available for growth as the growth-directed reserve flux $J_{E,G}$. In a single-reserve model, growth is straightforward: all of $J_{E,G}$ is transformed into new structural volume, with a transformation constant $[E_G]$ defining reserve mass needed per unit of structural volume produced.

When the model contains multiple reserve types, each indispensable for growth, the situation becomes more complicated. In effect the growth process now becomes a multiple substrate (reserves), one product (structural volume) transformation. The previously described synthesizing unit (SU) kinetics – developed for this type of transformation in particular – is applied here. The structural-volume-synthesis rate thus becomes a function of the arrival rates of the different reserves, i.e. $J_{E_i,G}$ for reserve E_i . For simplicity, the maximum rate of structural volume synthesis $J_{m,V}$ is taken to be infinitely high, and the reserve→SU binding probabilities $\rho_{E_i,V}$ are taken to equal 1. This also

improves consistency, for when applied to single-reserve growth, SU growth kinetics equal complete use of $J_{E_i,G}$, as defined for single reserve models previously. In the case of a two-reserve model, it results in the following kinetics for growth:

$$J_V = \frac{1}{\left(\frac{J_{E_1,G}}{y_{E_1,V}}\right)^{-1} + \left(\frac{J_{E_2,G}}{y_{E_2,V}}\right)^{-1} - \left(\frac{J_{E_1,G}}{y_{E_1,V}} + \frac{J_{E_2,G}}{y_{E_2,V}}\right)^{-1}}$$

As in any multiple-substrate transformation, part of the arriving substrate remains unused if another substrate is lacking: in synthesizing unit terms, a part is rejected. Reserves rejected at the growth synthesizing unit (flux $J_{E_i,R}$) DEB theory defines to be partly resorbed in the source reserve pool, and partly exudated. A fixed part κ_{E_i} of $J_{E_i,R}$ is defined to re-enter the reserve pool; leftovers are exudated. Exudation prevents an unrealistic infinite increase of reserve densities when another reserve is permanently lacking. It also accounts for natural phenomena like sugar exudation by aphids when their food contains little nitrogen. Note that J_V is limited, both through exudation-limited reserve densities, and growth-limited catabolic fluxes. Omitting $J_{m,V}$ in the SU kinetics therefore does not result in unlimited growth.

From individual to population

Although all concepts described previously relate to individuals, DEB theory does offer ways of extending these to populations. The entire population can be represented by a single DEB-individual, in effect an unstructured population. This approach does present one important problem, however: the assumption of isomorphism. A default DEB-individual grows isomorphically: its surface area is proportional to its volume^{2/3}. This is not the case for populations, for – when viewed as a collection of equally sized individuals – their surface area is proportional to volume¹ (V1-morphs in DEB theory). In reality of course, the volume-surface area dependency is a mixture of both: both the number of individuals and their size play a role. It can be shown, however, that a population becomes more like a V1-morph with increasing population size (assuming asynchronous division). Therefore most populations can safely be assumed to behave like a V1-morph.

Describing V1-morphs instead of isomorphs requires model modifications in every area where the volume-surface area relationship is involved. Because DEB models make extensive use of this relationship, this involves almost every part of the model, including the very start: food uptake. Since the maximum rate of food uptake was taken to be proportional to (structural) surface area, it now must be proportional to V . Instead of $V^{2/3} \cdot \{J_{X,m}\}$ we get $V \cdot [J_{X,m}]$, where $[J_{X,m}]$ is structural-volume-specific. The structural-volume-specific food uptake as used in reserve density kinetics then becomes:

$$[J_{X,A}] = [J_{m,X}] \cdot \frac{X}{X + X_{1/2}}$$

Because $[J_{X,A}]$ now is independent of V , the reserve kinetics should be modified for the weak homeostasis assumption to apply. Specifically the catabolic flux combined with dilution by growth should be independent of V . This then eliminates the $V^{-1/3}$ in the combined reserve outflow. Subsequently constant \dot{v}_E is replaced by \dot{k}_E , because of different dimensions: while the dimension of \dot{v}_E is $V^{1/3} \cdot t^{-1}$, the dimension of \dot{k}_E is t^{-1} . The differential for reserve densities and the catabolic flux thus become:

$$\frac{d}{dt}[M_E] = [J_{E,A}] - \dot{k}_E \cdot [M_E] + \kappa_E \cdot [J_{E,R}]$$

$$J_{E,C} = V \cdot [M_E] \cdot (\dot{k}_E - \dot{r}) \left(\dot{r} = \frac{1}{V} \cdot \frac{d}{dt} V \right)$$

Therefore we can define a structural-volume-specific catabolic flux, which is independent of V : $[J_{E,C}] = J_{E,C}/V$. This implies that the structural-volume-specific growth directed flux is independent of V too: $[J_{E,G}] = [J_{E,C}] - [J_{E,M}]$. In both single- and multiple-reserve models this results in a structure synthesis rate that is proportional to V . For single-reserve models this can easily be seen, for growth is proportional to $J_{E,G}$. The two-reserve growth function serves as an example for multiple reserve models:

$$\begin{aligned} J_V &= \frac{1}{\left(\frac{V \cdot [J_{E_1,G}]}{y_{E_1,V}} \right)^{-1} + \left(\frac{V \cdot [J_{E_2,G}]}{y_{E_2,V}} \right)^{-1} - \left(\frac{V \cdot [J_{E_1,G}]}{y_{E_1,V}} + \frac{V \cdot [J_{E_2,G}]}{y_{E_2,V}} \right)^{-1}} \\ &= V \cdot \frac{1}{\left(\frac{[J_{E_1,G}]}{y_{E_1,V}} \right)^{-1} + \left(\frac{[J_{E_2,G}]}{y_{E_2,V}} \right)^{-1} - \left(\frac{[J_{E_1,G}]}{y_{E_1,V}} + \frac{[J_{E_2,G}]}{y_{E_2,V}} \right)^{-1}} \end{aligned}$$

Accordingly population growth rate $\dot{r} = J_V/V$ is independent of V .

Interestingly enough the complete V1-morph model is independent of V when defined relative to structural volume. In biological terms: population size does not influence its behavior. When external circumstances are identical, both small and large populations will have the same structure-specific feeding rate, reserve densities (i.e. composition), growth rate, etc.

Model construction

This project aims to model the physiology of *Emiliana huxleyi*, with application in climate-related research in mind. The model's capacity to describe various forms of climate→organism interaction depends fully on the environmental variables included in the model. Based on interest and the availability of experimental data, we focus on the following:

- light intensity, which features prominently in numerous *Emiliana* experiments and thus allows for comparison of the model behavior with data.
- ambient CO₂, which allows for the model to be deployed in two areas of climate-related research: reconstruction of palaeoclimate CO₂ concentrations from *Emiliana* sediments, and predicting changes in the carbon cycle following the global CO₂ increase.
- 'nitrate', which in essence plays the role of a generic, possible limiting nutrient (i.e. the model lacks any specifics of nitrate metabolism) and allows for model deployment in ecosystem competition scenarios, for instance.

To determine the impact on the carbon cycle, inclusion of the following aspects of *Emiliana*'s behavior was considered indispensable:

- uptake and exudation of carbon species
- organic carbon per cell and CaCO₃ per cell, which allows for a link to sediment data through the inorganic : organic carbon ratio.
- population growth rate, which provides some measure of changes in abundance.

About physiology

To be able to give an accurate picture of *Emiliana*'s role in the carbon cycle, the model must include all major carbon fluxes the cell incorporates. Based on our need to distinguish imported carbon species, exported carbon species, fixed organic carbon and fixed CaCO₃, we classify *Emiliana*'s carbon fluxes as follows: CO₂ → organic carbon (photosynthesis), organic carbon → CO₂ (dark respiration) and HCO₃⁻ → CaCO₃/CO₂ (calcification).

Photosynthesis: CO₂ → organic carbon

Photosynthesis converts CO₂ into organic carbon compounds under influence of light. This is an intracellular process, occurring in the chloroplast. As the chloroplast lacks an inherent source of CO₂, it is dependent on diffusive entry of the solute from the cytoplasm. The cytoplasmic CO₂ concentration itself is in turn coupled to that of the environment: CO₂ can traverse the cell membrane reasonably well, causing the cytoplasmic CO₂ concentration to approximate that of the environment under most circumstances. Net CO₂ production (e.g. at night) will induce net diffusive CO₂ outflow, net CO₂ consumption will induce net diffusive CO₂ inflow.

The primary products of photosynthesis are carbohydrates: the cell's sole source of organic carbon. All other organic carbon-containing compounds, whether lipids, proteins or others, are produced from (a derivative of) photosynthetically-produced carbohydrates.

Dark respiration: organic carbon → CO₂

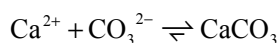
Dark respiration is a collective term for processes that produce CO₂. The major part of CO₂ production occurs in the mitochondrion, where energy (i.e. ATP) is generated from organic carbon compounds. For the most part, these compounds are derived from either carbohydrates or lipids. Next to basic respiration, various conversions of carbon-containing compounds may involve formation of some CO₂. Independent of the source, however, every molecule of CO₂ generated in dark respiration will have been formed from carbon that was originally fixed in photosynthesis.

All forms of respiration occur internally, and will thus increase the cytoplasmic CO₂ concentration. This will increase outward-directed CO₂ diffusion, causing either net CO₂ outflow when photosynthesis is absent or low, or reduced net inflow when photosynthesis is high.

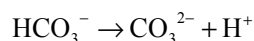
Calcification: HCO₃⁻ → CaCO₃/CO₂

Unlike photosynthesis and dark respiration, which are common to all algae, calcification is relatively rare. While it is found in numerous species, the mechanism employed by coccolithophorids (the group of which *E. huxleyi* is a member) is exceptional, in that it occurs internally in a highly controlled environment. Calcification takes place in a specialized organelle, derived from the Golgi. Here, CaCO₃ crystallizes onto a carbohydrate frame, which lays the basis for the intricate coccolith shape.

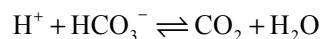
In general, the CaCO₃ crystallization reaction itself is thought to be a passive process. Unlike the far majority of biochemical reactions, which is enzyme-mediated, CaCO₃ crystallization would occur through standard chemical equilibria. Simply by generating high concentrations of Ca²⁺ and CO₃²⁻ inside the coccolith vesicle, the cell could force CaCO₃ precipitation:



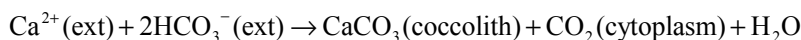
Thus, the main requirement for calcification in the coccolith vesicle is a continuous net influx of Ca²⁺ and CO₃²⁻. Clearly, as the cell lacks a source of either substrate, both will be imported in one form or another from the environment. Surprisingly, the CO₃²⁻ used in CaCO₃ formation has been shown to be derived from external HCO₃⁻, not carbonate (Brownlee et al., 1994). This has a significant advantage for the cell, as the external HCO₃⁻ concentration is well above that of CO₃²⁻, making import much easier. There is a side effect, however; as the imported HCO₃⁻ is converted into CO₃²⁻, the cell is left with H⁺:



Whether this conversion takes places in the cytoplasm or in the coccolith vesicle is unknown, but irrelevant for its impact. Even if it occurred in the coccolith vesicle, H⁺ would still end up in the cytoplasm, as the vesicle lacks an intrinsic proton sink. Thus, aside from producing CaCO₃, calcification is a source of acidification, which will initially be felt in the cytoplasm. This is also suggested by the fact that *Emiliana* cells have a lower internal pH than non-calcifying species of microalgae (Nimer et al., 1994). Free cytoplasmic H⁺ is almost non-existent; as soon as it becomes available, it will interact with the inorganic carbon equilibria, mostly in the following reaction:



Thus, the net calcification reaction is given by:



Thus, in essence, calcification acts as yet another source of CO₂. Like all cytoplasmic CO₂, that produced in this manner can suffer two fates: it will either diffuse outward, or be consumed in photosynthesis. Clearly, the latter use could be highly beneficial to the cell. Particularly at high light intensity – when CO₂ demand in photosynthesis is high and its diffusive entry from the environment is insufficient – calcification-produced CO₂ is likely to contribute significantly to photosynthesis. This has in fact been demonstrated in various *Emiliana* experiments that dealt with calcifying and non-calcifying strains: the former type was able to sustain almost double the photosynthetic rates of the latter.

A full, biochemically oriented overview of metabolic fluxes and transformations related to calcification can be found in Brownlee et al. (1994) and Anning et al. (1996).

Use of the DEB framework

To facilitate model comparison with results of – typically population-oriented – *Emiliana* experiments, the model was constructed to describe a population of *E. huxleyi*. This also allows us to provide some indication of its abundance, a characteristic that is of course in part responsible for *Emiliana*'s climate-influencing ability. For simplicity, the population is not modeled as a collection of distinct individuals (which would involve a great number of parameters, a complicated model setup and less transparent results), but rather as a single, summarizing individual: DEB theory's V1-morph. Model kinetics are V1-morph-specific, which becomes most visible in two areas: all aspects of the model are defined relative to the population's structure, including substance fluxes and the growth rate, and all surface-area-specific properties are replaced by structure-specific properties (which is possible because a V1-morph's surface area is proportional to its structure).

The *Emiliana* model differs in one aspect from the original DEB model: structural volume has been replaced by structural mass, i.e. the quantity of structural organic carbon. This replacement is possible because DEB theory assumes the composition of structure to be constant ('strong homeostasis'). A constant composition entails that volume is proportional to the quantity of the various chemical constituents. This implies that one can replace structural-volume-specific properties of the model by properties that are specific to the quantity of any structure constituent. Since this project focuses on carbon content of *Emiliana*, rather than the irrelevant and difficult to measure structural population volume, all occurrences of structural volume have been replaced by structural mass, specified as the amount of structural organic carbon. Because the original V1-morph model was defined relative to structural volume, replacing structural volume influences all parts of the model: fluxes and growth are now given relative to structural mass, surface-area-specific properties are replaced by structural-mass-specific properties, structural-volume-specific properties (e.g. maintenance requirement) are replaced by structural-mass-specific properties.

Model construction

To describe *Emiliana*'s physiology by DEB framework, we need to adhere to the DEB classification of compounds. This requires a clear distinction between nutrients, reserves and structure. Nutrients are taken up, and transformed into reserves. Reserve outflow drives organism maintenance, after which the reserve surplus, if any, becomes available to structure synthesis.

The carbon flux overview presented above must be placed into this context. Photosynthesis can be well described as a process that transforms nutrients into a carbon reserve. Dark respiration, on the other hand, is an obligatory carbon-reserve-depleting process, which in context of the DEB framework is well described as combination of size-dependent organism maintenance, and growth-dependent energy consumption. Calcification does take up nutrients, as it requires both Ca²⁺ and HCO₃⁻, but unlike photosynthesis, its most conspicuous product, CaCO₃, is not required for further metabolism. On the other hand, its CO₂ producing efforts can be most relevant, as it is likely to significantly enhance photosynthesis. Thus, it is well described as a process supplying additional CO₂ to photosynthesis.

Carbon pathways

Photosynthesis is modeled as a synthesizing unit transformation, i.e. taken comparable to an enzyme-mediated process in which substrate binding is irreversible. The rate of photosynthesis is assumed to be controlled by the availability of two 'substrates': CO₂ and light (implicitly, any other required

substrates are assumed abundant). Both are required in order to synthesize the main product: a carbon reserve, referred to as CH₂O. Note that, despite the name, the composition of the CH₂O reserve is not restricted to carbohydrates; as it is merely defined to be built from CO₂ and a certain amount of light, it may just as well contain lipids and other forms of organic carbon. That would merely increase the required amount of light per unit of reserve. The only requirement for the reserve is that its composition is constant.

As any synthesizing unit mediated process, photosynthesis is restricted by a maximum rate. This maximum rate is assumed proportional to the structural mass of the modeled ‘individual’, or – as it in fact represents an entire population of *Emiliana* – the number of individuals in the population. Thus, the structural-mass-specific rate of photosynthesis can be given by:

$$j_{\text{CH}_2\text{O},A} = \frac{1}{j_{m,\text{CH}_2\text{O}}^{-1} + j'_{\text{light},\text{CH}_2\text{O}}^{-1} + j'_{\text{CO}_2,\text{CH}_2\text{O}}^{-1} - (j'_{\text{light},\text{CH}_2\text{O}} + j'_{\text{CO}_2,\text{CH}_2\text{O}})^{-1}}$$

All fluxes are structural-mass-specific (identifier $j_{x,y}$, rather than $J_{x,y}$), with dimension mole CH₂O per C-mole structure per day. $j_{m,\text{CH}_2\text{O}}$ is a constant, representing the maximum rate of photosynthesis. $j'_{\text{light},\text{CH}_2\text{O}}$ and $j'_{\text{CO}_2,\text{CH}_2\text{O}}$ represent effective arrival rates of light and CO₂, respectively. The latter two are functions of the true arrival rate $j_{\text{substrate},\text{CH}_2\text{O}}$, the substrate-per-CH₂O yield $y_{\text{substrate},\text{CH}_2\text{O}}$ and the binding probability $\rho_{\text{substrate},\text{CH}_2\text{O}}$ of the substrate with respect to the SU:

$$j'_{\text{light},\text{CH}_2\text{O}} = \frac{\rho_{\text{light},\text{CH}_2\text{O}}}{y_{\text{light},\text{CH}_2\text{O}}} \cdot j_{\text{light},\text{CH}_2\text{O}}$$

$$j'_{\text{CO}_2,\text{CH}_2\text{O}} = \frac{\rho_{\text{CO}_2,\text{CH}_2\text{O}}}{y_{\text{CO}_2,\text{CH}_2\text{O}}} \cdot j_{\text{CO}_2,\text{CH}_2\text{O}} = \frac{\rho_{\text{CO}_2,\text{CH}_2\text{O}}}{1} \cdot j_{\text{CO}_2,\text{CH}_2\text{O}}$$

As we assume all organic carbon to be produced from CO₂, the CO₂-per-CH₂O yield $y_{\text{CO}_2,\text{CH}_2\text{O}}$ can safely be set to 1.

Light arrival at the photosynthesizing unit is taken proportional to the external light intensity $\{J_{\text{light}}\}$, specified in $\mu\text{mol photons per m}^2$ per second. In addition it is taken proportional to structural mass, i.e. the number of individuals in the population. Thus, the light availability per individual is independent of population size. The structural-mass-specific light arrival at the CH₂O SU is given by:

$$j_{\text{light},\text{CH}_2\text{O}} = \alpha \cdot \{J_{\text{light}}\}$$

$j_{\text{light},\text{CH}_2\text{O}}$ appears only in $j'_{\text{light},\text{CH}_2\text{O}}$. This implies that α only occurs in conjunction with $\rho_{\text{light},\text{CH}_2\text{O}}$ and $y_{\text{light},\text{CH}_2\text{O}}$. These three constants can therefore be collapsed into a single constant γ_{light} , in effect representing the potential CH₂O yield per external light intensity per present structural mass (potential because photosynthesis is restricted by a maximum rate, and by a possible lack of CO₂).

CO₂ arrival at the photosynthesizing unit is more complicated than light arrival, because multiple sources contribute to it. Diffusion, dark respiration and calcification each supply some CO₂. A biochemical approach would most likely account for this by including an internal CO₂ pool, through which the various sources and sinks could interact. However, this is preferably avoided, as it would require an additional state variable. Instead, $j_{\text{CO}_2,\text{CH}_2\text{O}}$ is simply taken to be combination of inward CO₂ diffusion $j_{\text{CO}_2,\text{dif},\text{CH}_2\text{O}}$, CO₂ production in respiration $j_{\text{CO}_2,\text{resp},\text{CH}_2\text{O}}$ and CO₂ production in calcification $j_{\text{CO}_2,\text{calc},\text{CH}_2\text{O}}$:

$$j_{\text{CO}_2, \text{CH}_2\text{O}} = j_{\text{CO}_2, \text{dif}, \text{CH}_2\text{O}} + j_{\text{CO}_2, \text{resp}, \text{CH}_2\text{O}} + j_{\text{CO}_2, \text{calc}, \text{CH}_2\text{O}}$$

CO₂ arrival through diffusion is taken proportional to the external CO₂ concentration C_{CO_2} and structural mass, with proportionality constant γ_{CO_2} :

$$j_{\text{CO}_2, \text{ext}, \text{CH}_2\text{O}} = \gamma_{\text{CO}_2} \cdot C_{\text{CO}_2}$$

CO₂ arrival from respiration equals the combined CO₂ production rates of DEB maintenance and growth processes. The DEB framework specifies substance fluxes related to maintenance and growth as the rate of disappearance (resp. $J_{\text{substance}, M}$ and $J_{\text{substance}, G}$). Consequently, the rate at which respiration produces CO₂ is the sum of $J_{\text{CO}_2, M}$ and $J_{\text{CO}_2, G}$, but with opposite sign. When made structural-mass-specific, this amounts to:

$$j_{\text{CO}_2, \text{resp}, \text{CH}_2\text{O}} = -(j_{\text{CO}_2, M} + j_{\text{CO}_2, G})$$

Actual values of $j_{\text{CO}_2, M}$ and $j_{\text{CO}_2, G}$ are determined by the specifics of maintenance and growth, and can be found below.

CO₂ arrival from calcification is taken proportional to the external HCO₃⁻ concentration $C_{\text{HCO}_3^-}$ and the structural mass, with proportionality constant $\gamma_{\text{HCO}_3^-}$:

$$j_{\text{CO}_2, \text{calc}, \text{CH}_2\text{O}} = \gamma_{\text{HCO}_3^-} \cdot C_{\text{HCO}_3^-}$$

Note that calcification is not influenced by the availability of other substrates (e.g. Ca²⁺); these are assumed abundant.

Photosynthesis can never make full use of offered substrates. Its production rate, and thereby the rate of substrate consumption, is restricted by the maximum rate of CH₂O production $j_{m, \text{CH}_2\text{O}}$, and by potentially low arrival rates of CO₂ and light. Hence, part of the arriving substrate fluxes is rejected. For all substrates, this rejected flux does not contribute any further to photosynthesis: it disappears from the scope of the model. The interpretation of this disappearance varies per type of substrate: rejected light is assumed to pass through or dissipate at heat, rejected CO₂ that originated from diffusion or respiration is assumed to disappear through outward diffusion. However, to establish the often observed correlation between photosynthesis and calcification, we assume rejected calcification-related CO₂ to never have been produced by calcification, i.e. to result in outward HCO₃⁻ diffusion. Calcification therefore only occurs if CO₂ available through calcification is actually used in photosynthesis: calcification answers to photosynthesis demand only.

From the rate of photosynthesis we can derive the uptake rate of CO₂ and HCO₃⁻. The net CO₂ uptake is specified by the difference between CO₂ inflow ($j_{\text{CO}_2, \text{dif}, \text{CH}_2\text{O}}$) and outflow (the part of $j_{\text{CO}_2, \text{dif}, \text{CH}_2\text{O}}$ and $j_{\text{CO}_2, \text{resp}, \text{CH}_2\text{O}}$ rejected at the photosynthesizing unit). CO₂ produced in calcification is per definition fully consumed in photosynthesis, and therefore not directly of influence for CO₂ uptake. The ratio at which various CO₂ sources are rejected is taken to equal the ratio at which they contribute to CO₂ arrival. Thus, the net structural-mass-specific rate of CO₂ uptake is given by:

$$\begin{aligned} j_{\text{CO}_2, \text{uptake}} &= j_{\text{CO}_2, \text{dif}, \text{CH}_2\text{O}} - \frac{j_{\text{CO}_2, \text{dif}, \text{CH}_2\text{O}} + j_{\text{CO}_2, \text{resp}, \text{CH}_2\text{O}}}{j_{\text{CO}_2, \text{CH}_2\text{O}}} \cdot (j_{\text{CO}_2, \text{CH}_2\text{O}} - j_{\text{CH}_2\text{O}, A}) \\ &= \frac{j_{\text{CO}_2, \text{dif}, \text{CH}_2\text{O}} + j_{\text{CO}_2, \text{resp}, \text{CH}_2\text{O}}}{j_{\text{CO}_2, \text{CH}_2\text{O}}} \cdot j_{\text{CH}_2\text{O}, A} - j_{\text{CO}_2, \text{resp}, \text{CH}_2\text{O}} \end{aligned}$$

HCO₃⁻ uptake is related to calcification only. The rate of calcification is defined as the rate at which photosynthesis consumes CO₂ that is available through calcification. The rate at which photosynthesis consumes CO₂ is equal to $j_{\text{CH}_2\text{O},A}$. The ratio at which various CO₂ sources contribute to photosynthesis is taken equal to the ratio at which they contribute to CO₂ arrival. Hence the net structural-mass-specific rate of HCO₃⁻ uptake (which is twice the rate of CO₂ production by calcification, based on calcification stoichiometry) is given by:

$$j_{\text{HCO}_3^- \text{ uptake}} = 2 \cdot \frac{j_{\text{CO}_2 \text{ calc, CH}_2\text{O}}}{j_{\text{CO}_2, \text{CH}_2\text{O}}} \cdot j_{\text{CH}_2\text{O},A}$$

All photosynthesis-produced CH₂O is initially incorporated in a CH₂O reserve pool. Following DEB theory, the differential equation for reserve density and the structural-mass-specific catabolic rate are given by:

$$\frac{d}{dt} m_{\text{CH}_2\text{O}} = j_{\text{CH}_2\text{O},A} - \dot{k}_{\text{CH}_2\text{O}} \cdot m_{\text{CH}_2\text{O}} + \kappa_{\text{CH}_2\text{O}} \cdot j_{\text{CH}_2\text{O},R}$$

$$j_{\text{CH}_2\text{O},C} = m_{\text{CH}_2\text{O}} \cdot (\dot{k}_{\text{CH}_2\text{O}} - \dot{r})$$

Part of the catabolic flux is used to satisfy the structural-mass-specific maintenance requirement $j_{\text{CH}_2\text{O},M}$. CH₂O left over becomes available for growth:

$$j_{\text{CH}_2\text{O},G} = j_{\text{CH}_2\text{O},C} - j_{\text{CH}_2\text{O},M}$$

CH₂O consumed by maintenance is taken to be converted into CO₂. Thus, maintenance-related CO₂ consumption is given by:

$$j_{\text{CO}_2,M} = -j_{\text{CH}_2\text{O},M}$$

Note: no other reserve will be included that contain carbon. Thus, CH₂O is the only maintenance-related source of CO₂.

An additional nutrient dependency

To extend the applicability of the model, another possibly limiting nutrient has been included in the model. This allows the model to describe situations in which behavior is influenced by input variables besides light intensity and the concentrations of CO₂ and HCO₃⁻. In the model this nutrient is represented by nitrate: NO₃⁻.

Uptake of nitrate is assumed to occur through active transport only. Therefore the uptake rate can be described by standard DEB food uptake kinetics, rendering a hyperbolic relationship between nitrate uptake $j_{\text{NO}_3^-,A}$ and ambient nitrate concentration $C_{\text{NO}_3^-}$:

$$j_{\text{NO}_3^-,A} = j_{m,\text{NO}_3^-} \cdot \frac{C_{\text{NO}_3^-}}{C_{\text{NO}_3^-} + C_{\frac{1}{2},\text{NO}_3^-}}$$

Like photosynthesis, nitrate uptake is restricted by a maximum rate, which is taken to be structural-mass-specific: j_{m,NO_3^-} . $C_{\frac{1}{2},\text{NO}_3^-}$ represents the external nitrate concentration at which nitrate uptake occurs at half of its maximum rate.

After uptake, nitrate is first incorporated in a reserve pool. This allows for temporary survival in low-nitrate environments. In addition, this reserve can influence the average composition of the population: depending on ambient nitrate concentration, the nitrate reserve can be a negligible to substantial part of the total content. The nitrate reserve follows standard DEB reserve kinetics, which means the differential equation for nitrate reserve density and the catabolic flux are given by:

$$\frac{d}{dt}m_{\text{NO}_3^-} = j_{\text{NO}_3^-,A} - \dot{k}_{\text{NO}_3^-} \cdot m_{\text{NO}_3^-} + \kappa_{\text{NO}_3^-} \cdot j_{\text{NO}_3^-,R}$$

$$j_{\text{NO}_3^-,C} = m_{\text{NO}_3^-} \cdot (\dot{k}_{\text{NO}_3^-} - \dot{r})$$

After paying the structural-mass-specific maintenance cost $j_{\text{NO}_3^-,M}$, the structural-mass-specific growth-directed nitrate flux is given by:

$$j_{\text{NO}_3^-,G} = j_{\text{NO}_3^-,C} - j_{\text{NO}_3^-,M}$$

Growth: synthesis of structural mass

As in all DEB-based models, all substance pathways end with the synthesis of new structure, which in this case corresponds to population growth. Growth is specified as synthesis of structural mass. Here, it is taken to depend on the availability of two substrates: the CH₂O reserve and the NO₃⁻ reserve. This assumes any other substrates are abundant and not growth limiting. Following DEB theory, synthesis of structural mass is modeled as a slightly modified synthesizing unit transformation (no maximum rate, binding probabilities of 1), and thus dependent on growth-directed substrate fluxes ($j_{\text{CH}_2\text{O},G}$, $j_{\text{NO}_3^-,G}$), and on the reserve-per-structural-mass yields ($y_{\text{CH}_2\text{O},V}$, $y_{\text{NO}_3^-,V}$). The population growth rate (structural mass synthesized per structural mass present, $dM_V/dt \cdot M_V^{-1}$) is given by:

$$\dot{r} = \frac{1}{\left(\frac{j_{\text{CH}_2\text{O},G}}{y_{\text{CH}_2\text{O},V}}\right)^{-1} + \left(\frac{j_{\text{NO}_3^-,G}}{y_{\text{NO}_3^-,V}}\right)^{-1} - \left(\frac{j_{\text{CH}_2\text{O},G}}{y_{\text{CH}_2\text{O},V}} + \frac{j_{\text{NO}_3^-,G}}{y_{\text{NO}_3^-,V}}\right)^{-1}}$$

Note that this is an implicit description of growth, as both growth-directed fluxes depend on \dot{r} through their respective catabolic fluxes ($j_{\text{CH}_2\text{O},C}$, $j_{\text{NO}_3^-,C}$).

In most circumstances only part of the growth directed reserve fluxes is actually used for growth. Lack of one substrate prevents growth, and thereby the use of the other. A substrate flux is used in full only if the other substrate is abundant (essentially, if $j_{\text{substrate},G} \rightarrow \infty$). Since the used part of a reserve flux corresponds to structural mass increase multiplied by the yield constant, the fluxes of unused (rejected) reserves are given by:

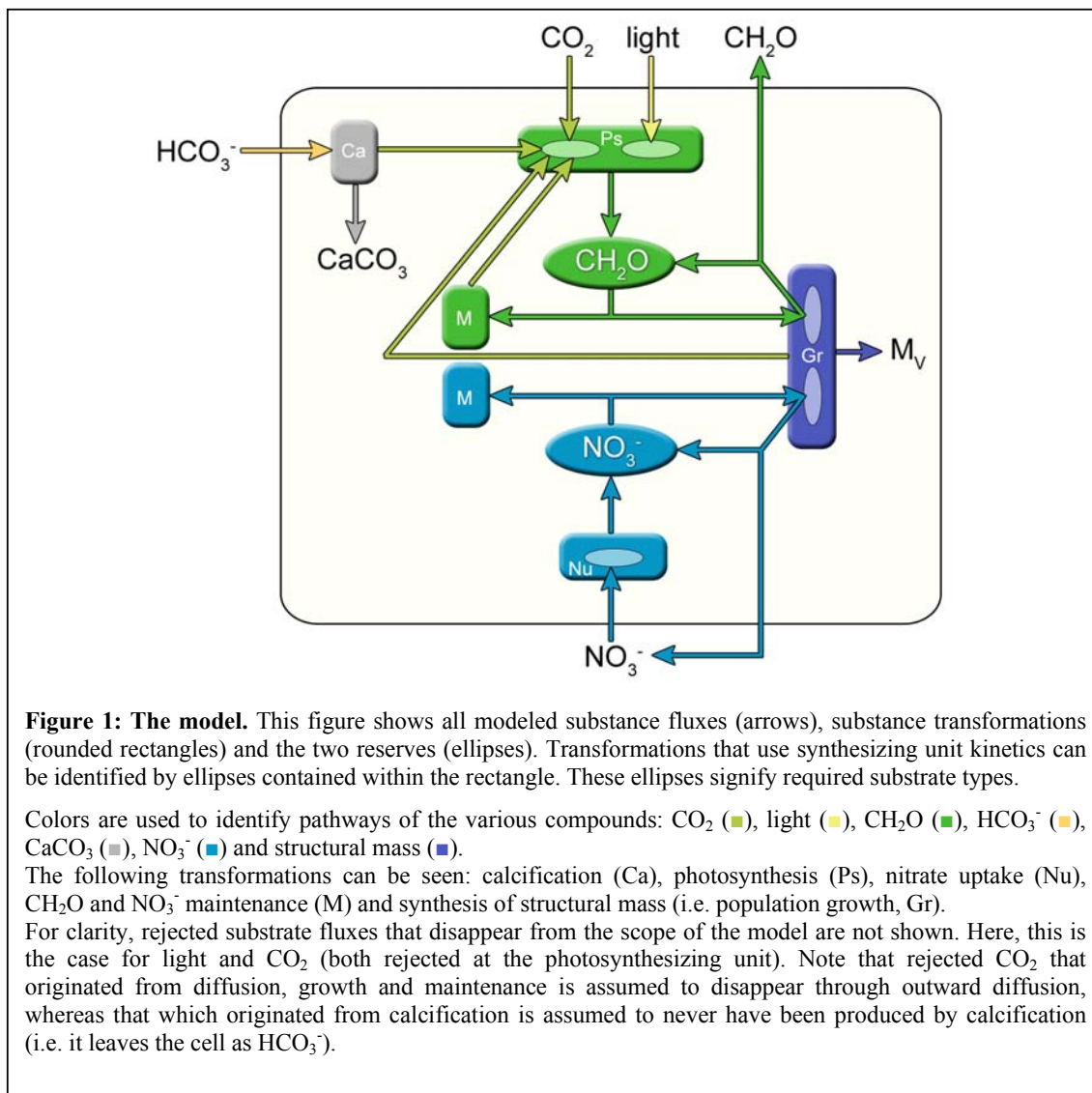
$$j_{\text{CH}_2\text{O},R} = j_{\text{CH}_2\text{O},G} - y_{\text{CH}_2\text{O},V} \cdot \dot{r}$$

$$j_{\text{NO}_3^-,R} = j_{\text{NO}_3^-,G} - y_{\text{NO}_3^-,V} \cdot \dot{r}$$

As defined by DEB and as signified by the previously described reserve kinetics, part of these rejected fluxes is reincorporated in the reserve pool. The parts returning to the CH₂O and NO₃⁻ reserve pools are defined by $\kappa_{\text{CH}_2\text{O}}$ and $\kappa_{\text{NO}_3^-}$, respectively. Subsequently, what is left of the rejected reserve fluxes is exudated.

Only part of the carbon consumed in growth will end up in structural carbon-containing compounds. Per $y_{\text{CH}_2\text{O},V}$ mole CH₂O consumed, one mole of structural carbon is generated. The additional CH₂O will be used to generate the energy required for growth, and is assumed to be fully converted into CO₂. Thus, we can specify the following rate of (negative) growth-related CO₂ consumption:

$$j_{\text{CO}_2,G} = -\dot{r} \cdot (y_{\text{CH}_2\text{O},V} - 1)$$



Methods of analysis

The model was designed to be applied to scenarios of global climate change, particularly those dealing with changes in the ambient CO₂ concentration. These are relatively slow processes: the time required for even the slightest change will far exceed the lifespan of an *Emiliana* individual. Experiments have shown *Emiliana* populations to enter steady state (i.e. constant growth rate, constant cell characteristics) within five days, even following severe changes in major environmental parameters. Considering that climate change is far less abrupt, it is more than likely that during the process, populations are continuously in steady state. Therefore, model analysis focuses on steady state solving, rather than integration.

First and foremost, the model's behavior is compared with real-world data. The model was fitted to the results of an experiment that deals with the effect of light limitation on population growth and calcification. These aspects of *Emiliana* are well studied, and the quality of the model's fit can provide some indication of its applicability.

Steady state analysis

Before diving into steady state solving mechanisms, it is important to realize what is meant by 'steady state'. Contrary to what one might think, it does not necessarily imply a constant population size. The complete *Emiliana* model is independent of structural mass (i.e. population size) when defined relative to structural mass. Hence, given the same environment, a population with a size of, say, 2, will equal 2 separate populations of 1, both in composition and behavior. This implies no intrinsic maximum population size is present. Since we also assume ambient 'nutrient' availability (light, CO₂, HCO₃⁻, NO₃⁻) to be independent of uptake by the population, it is clear that steady state does not equal a growth rate of zero. Rather, when kept in a constant environment long enough, the reserve densities (the amount of reserves per individual) will become constant, resulting in a constant population growth rate. At that point, reserve synthesis (through food uptake) will equal the sum of reserve use in maintenance/growth and reserve outflow. Summarizing, steady state is defined in this context as a situation in which the reserve densities of both CH₂O and NO₃⁻ are constant, and the population grows exponentially.

The above definition implies that, at steady state, the following should be true:

$$\frac{d}{dt}m_{\text{CH}_2\text{O}} = 0$$

$$\frac{d}{dt}m_{\text{NO}_3^-} = 0$$

These conditions would suffice to determine the values of $m_{\text{CH}_2\text{O}}$ and $m_{\text{NO}_3^-}$ (and thus to fully describe the steady state), if all model variables were explicitly defined. This is not the case, however: the growth rate \dot{r} is described by an implicit expression only. Thus, a complete description of steady state requires not only the finding of the values of reserve densities, but also the value of \dot{r} . To achieve this, we make use of the fact that the value of \dot{r} , like those of reserve densities, is bound by a condition: under all circumstances, it is described by:

$$\dot{r} = \frac{1}{\left(\frac{j_{\text{CH}_2\text{O},G}}{y_{\text{CH}_2\text{O},V}}\right)^{-1} + \left(\frac{j_{\text{NO}_3^-,G}}{y_{\text{NO}_3^-,V}}\right)^{-1} - \left(\frac{j_{\text{CH}_2\text{O},G}}{y_{\text{CH}_2\text{O},V}} + \frac{j_{\text{NO}_3^-,G}}{y_{\text{NO}_3^-,V}}\right)^{-1}}$$

From now on, I use $f(\dot{r})$ as identifier for the right part of this expression.

Combined, solving steady state requires finding the values of three variables, $m_{\text{CH}_2\text{O}}$, $m_{\text{NO}_3^-}$ and \dot{r} , which are restricted by three conditions: $dm_{\text{CH}_2\text{O}}/dt=0$, $dm_{\text{NO}_3^-}/dt=0$ and $\dot{r}=f(\dot{r})$. This is a problem that can typically easily be solved by a root solving routine like Newton's, requiring n conditions to find the value of n variables.

In this specific case, additional simplification is possible. For both reserve densities, an 'explicit' description can be derived. Below, this is shown for a generic *reserve* compound. The differential equation for the reserve density should equal zero, i.e.:

$$\frac{d}{dt}m_{\text{reserve}} = j_{\text{reserve},A} - \dot{k}_{\text{reserve}} \cdot m_{\text{reserve}} + \kappa_{\text{reserve}} \cdot j_{\text{reserve},R} = 0$$

The rejected flux $j_{\text{reserve},R}$ can be rewritten as follows:

$$j_{\text{reserve},R} = m_{\text{reserve}} \cdot (\dot{k}_{\text{reserve}} - \dot{r}) - j_{\text{reserve},M} - \dot{r} \cdot y_{\text{reserve},V}$$

When this expression is inserted in dm_{reserve}/dt , the following expression for reserve density at steady state can be found:

$$m_{\text{reserve}} = \frac{j_{\text{reserve},A}/\kappa_{\text{reserve}} - j_{\text{reserve},M} - \dot{r} \cdot y_{\text{reserve},V}}{\dot{k}_{\text{reserve}} \cdot (1/\kappa_{\text{reserve}} - 1) + \dot{r}}$$

For the carbohydrate- and nitrate reserves, this comes to:

$$m_{\text{CH}_2\text{O}} = \frac{j_{\text{CH}_2\text{O},A}/\kappa_{\text{CH}_2\text{O}} - j_{\text{CH}_2\text{O},M} - \dot{r} \cdot y_{\text{CH}_2\text{O},V}}{\dot{k}_{\text{CH}_2\text{O}} \cdot (1/\kappa_{\text{CH}_2\text{O}} - 1) + \dot{r}}$$

$$m_{\text{NO}_3^-} = \frac{j_{\text{NO}_3^-,A}/\kappa_{\text{NO}_3^-} - j_{\text{NO}_3^-,M} - \dot{r} \cdot y_{\text{NO}_3^-,V}}{\dot{k}_{\text{NO}_3^-} \cdot (1/\kappa_{\text{NO}_3^-} - 1) + \dot{r}}$$

Note that these are not truly explicit descriptions, as both depend on \dot{r} , which in turn depends on $m_{\text{CH}_2\text{O}}$ and $m_{\text{NO}_3^-}$. When these descriptions for the reserve density in steady state are inserted in $\dot{r}=f(\dot{r})$, our 3 variables/3 equations problem is reduced to one of 1 variable/1 equation.

Unfortunately, as $f(\dot{r})$ is a very complex function of \dot{r} , multiple valid solutions for \dot{r} may exist. In other words: there may exist multiple, different steady states at a given set of parameters. Using Wolfram Corporation's Mathematica 4, $\dot{r}=f(\dot{r})$ has been shown to be transformable into $g(\dot{r})=0$ with $g(\dot{r})$ being an 11th order polynomial in \dot{r} . For such a polynomial, 11 solutions of \dot{r} exist at which the function equals zero. These can be either complex or non-complex. Thus, there might be up to 11 different, valid (i.e. non-complex) solutions for \dot{r} with certain parameter sets. Whether this actually occurs it strictly dependent on the choice of parameter values; as all parameters are constrained by certain bounds (e.g. none should be < 0), the number of valid solutions may well be significantly reduced.

The model in steady state was analyzed using a custom implementation of the Newton-algorithm, (Burden & Faires, 1985). This algorithm attempts to minimize n user-supplied functions through the varying of n user-selected variables. The user is responsible for providing fitting initial values for every variable.

At every iteration, an evaluation of the partial derivatives of every function is performed. For each variable x_i and function $f_i(x_1, \dots, x_n)$, these derivatives were approximated numerically by calculating the difference between $f_i(x_i + 10^{-7})$ and $f_i(x_i - 10^{-7})$, and dividing by $2 \cdot 10^{-7}$. The algorithm requires inversion of the Jacobian matrix at every iteration. For this purpose, a custom implementation of the Gaussian matrix-inversion algorithm (Burden & Faires, 1985) was provided. The maximum number of iterations for the Newton algorithm was set at 100, but never attained in any situation tried.

Before steady states were estimated for the full model, it was tested whether the more generic two-reserves-for-growth DEB model (where food uptake is independent of growth) allowed for multiple steady states. In theory, up to 3 steady state could exist, as $f(\dot{r}) - \dot{r}$ in that case can be transformed into a 3rd order polynomial.

For numerous set of parameter values, and different initial estimates for \dot{r} , I estimated steady state values of \dot{r} using the Newton algorithm (with $f(\dot{r}) - \dot{r}$ set as the function to minimize). Food uptake was neglected, and both reserve densities were considered parameters. For every parameter, 3 values were tried: an initial estimate p , $10 p$ and $0.1 p$. The parameters were varied independently of each other, resulting in 3^{11} unique parameter sets. In addition, 101 different initial estimates for \dot{r} were used, ranging from -5 up to 5, with steps of 0.1 between.

Initially, steady state estimation proved difficult: numerous times, the maximum number of iterations of the Newton algorithm was exceeded, or the Jacobian matrix became singular. These problems were eliminated, however, when the Newton algorithm was set to minimize the 3rd order polynomial transformation of $f(\dot{r}) - \dot{r}$, rather than the function itself.

For many parameter sets, different solutions of \dot{r} were obtained at different initial estimates of \dot{r} . This would suggest the existence of multiple valid steady states. However, for every one of these cases, all, or all but one of these solutions could be discarded based on other conditions, specifically the requirement that $j_{\text{CH}_2\text{O},G}$ and $j_{\text{NO}_3^-,G}$ each should be ≥ 0 . In other words: if a population is proclaimed dead when it is unable to pay maintenance costs, we never find more than one valid steady state. Note a total lack of steady states is indeed to be expected for certain parameter sets, as the maintenance requirement can exceed the capacity of reserve rendering processes.

These results strongly suggests that at maximum, only one steady state exists for any given set of parameters, provided the their values lie within realistic ranges¹. Hence, the Newton algorithm, which would otherwise be unsuitable because of its inability to reliably trace multiple valid values of \dot{r} , seems well suited for this type of steady state analysis. Analysis of the results shows that an initial estimate of $\dot{r} = 0$ will in all tested circumstances cause convergence of the algorithm around the valid steady state, providing one exists. Therefore, in all further steady state analyses the initial value of \dot{r} provided to the Newton algorithm was set to 0.

Data fitting

To allow for the model's behavior to be compared to results of experiments, the steady state solving algorithm was coupled to a Simplex parameter estimating routine. This algorithm attempts to minimize a user-specified function $f(p_1, \dots, p_n)$ by varying the value of n user-selected parameters p_1, \dots, p_n . The algorithm maintains an internal list of $n+1$ different parameter sets, which are initially supplied by the user. At every iteration an optimal set of parameters is predicted based on the value of $f(p_1, \dots, p_n)$ at all current parameter sets. This newfound set replaces the parameter set that produced the highest value of $f(p_1, \dots, p_n)$.

¹ Note: no additional testing was done to check whether the full model (in which food uptake depends on the growth rate) allowed for multiple steady states. In theory, 9 steady states (two out of 11 were eliminated) are possible.

To obtain an optimal fit for multiple datasets, $f(p_1, \dots, p_n)$ was chosen a weighted sum-of-squares function. This function equals the sum of weighted sum-of-squares functions for every dataset individually:

$$f(p_1, \dots, p_n) = f_{wss, dataset 1}(p_1, \dots, p_n) + f_{wss, dataset 2}(p_1, \dots, p_n) + \dots$$

For a single dataset, the weighted sum-of-squares function equals the following, given the datasets contains multiple (X_i, Y_i) coordinates:

$$f_{wss}(p_1, \dots, p_n) = \frac{\sum_{i=1}^{n_p} (Y_i - z_i(X_i, p_1, \dots, p_n))^2}{\bar{Y}}$$

Herein, n_p represents the number of points in the dataset, $z_i(X_i, p_1, \dots, p_n)$ represents the Newton estimate of variable Y , and \bar{Y} represents the average value of Y for all data points combined (i.e. the weighing factor). Note that different datasets may describe relationships between different variables; i.e. one could combine a dataset describing light intensity vs. population growth with one describing nitrate concentration vs. calcification.

The required initial $n+1$ parameter sets were built from one set of parameter estimates. This base set was supplied at the start of the estimation, and served as the basis for all others. Set 1 equals the base set. Set 2 equals the base set, except for the fact that p_1 was increased by 25 %. Set 3 equals the base set, except for the fact that p_2 was increased by 25 %. Etc.

The simplex routine was set to perform 5000 iterations, with no evaluation of intermediate results (e.g. tolerance checking). However, monitoring of several runs showed that no significant changes in estimated parameter values occurred after 3000 iterations.

Results and discussion: model I

Comparison with data

Historically, a major part of coccolithophorid research has focused on the relationship between light availability and growth/calcification. The model was designed to fit into this line of research, and should therefore adequately describe commonly observed trends in this field.

I fitted the model to data obtained from batch growth experiments (van Bleijswijk, 1996). In these experiments, *Emiliana* cultures were kept at various light intensities for a period of 3 weeks. Individual cultures were diluted when their density exceeded 10⁴ cells.ml⁻¹, thus ensuring that the population's impact on its environment (through depletion of nutrients, a decrease in light intensity, aggregation of waste products) was minimal. This allowed to maintain a constant growth rate during the full length of the experiment. Hence, the behavior of the populations should be well described by the model when it is in steady state.

The model was fitted simultaneously to the following two datasets:

- light intensity vs. the rate of organic carbon (OC) synthesis per present OC. As the populations are in steady state, the CH₂O reserve density of newly synthesized matter is identical to that of the standing population. Thus, the rate of OC synthesis per standing OC is identical to the population growth rate:

$$\frac{\text{OC synthesis}}{\text{OC present}} = \frac{\dot{r} \cdot (1 + m_{\text{CH}_2\text{O}})}{1 + m_{\text{CH}_2\text{O}}} = \dot{r}$$

where \dot{r} and $m_{\text{CH}_2\text{O}}$ depend on light intensity.

- light intensity vs. the rate of inorganic carbon (CaCO₃) synthesis per present OC. In the model, this rate is given by:

$$\frac{\text{CaCO}_3 \text{ synthesis}}{\text{OC present}} = \frac{j_{A,\text{CH}_2\text{O}} \cdot j_{\text{CO}_2,\text{calc},\text{CH}_2\text{O}} / j_{\text{CO}_2,\text{CH}_2\text{O}}}{1 + m_{\text{CH}_2\text{O}}}$$

where $j_{\text{CH}_2\text{O},A}$, $m_{\text{CH}_2\text{O}}$ and $j_{\text{CO}_2,\text{CH}_2\text{O}}$ each depend on light intensity.

From these synthesis rates, the molar inorganic carbon to organic carbon ratio was calculated. This ratio is identical for both cell contents and synthesis rates, as the population is in steady state. The adequacy of the model's description of the IC : OC ratio served as an additional criterion in determining the model's usability.

Only parameters expected to affect light – carbon synthesis interaction were estimated. This excludes all parameters related to the nitrate pathway: as all nutrients were kept at optimal availability, nitrate (or any other nutrient not explicitly included in the model) should not affect the model's behavior. j_{m,NO_3^-} and $k_{\text{NO}_3^-}$ were set to a high values to ensure ample nitrate is present throughout the model, whereas other nitrate-related parameters were simply set to generic values. The effect of nitrate abundance is that growth cannot be nitrate-limited (i.e. $j_{\text{NO}_3^-,G} \rightarrow \infty$). Therefore, no CH₂O arriving at the growth SU will be rejected. The value of $\kappa_{\text{CH}_2\text{O}}$ consequently cannot influence the model's behavior, and was not estimated.

Table 1 presents an overview of all parameter values. Values of the input variables of the model were set to $C_{\text{CO}_2} = 15 \mu\text{M}$, $C_{\text{HCO}_3^-} = 2000 \mu\text{M}$ and $C_{\text{NO}_3^-} = 50 \mu\text{M}$ (van Bleijswijk, 1996).

Figures 2 to 4 present the results. The final parameter estimates as produced by the Simplex algorithm are included in table 1. However, these values are only provided to allow for complete reproduction of the results; by no means do the limited datasets constrain the parameters. Even the slightest change to the initial estimates resulted in vastly different final estimates, though the fitted curves appeared identical.

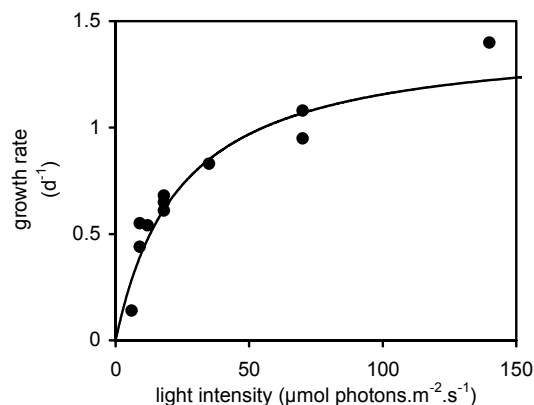


Figure 2: population growth as a function of light intensity.

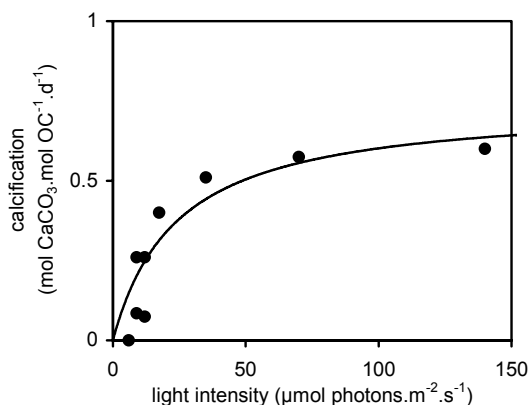


Figure 3: calcification as a function of light intensity.

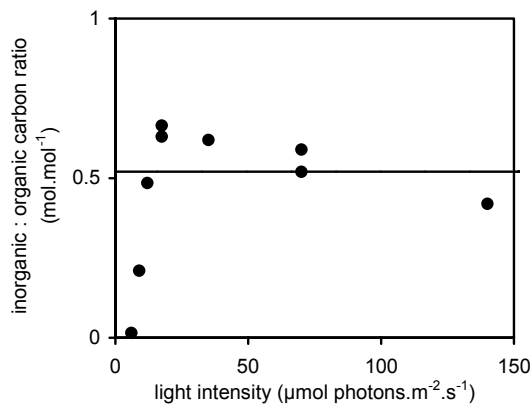


Figure 4: the inorganic carbon : organic carbon ratio as a function of light intensity. This statistic is calculated by dividing the rate of calcification by the rate of organic carbon production (both for the data and the model).

parameter	unit	initial estimate	final estimate
j_{m,CH_2O}	mol CH ₂ O.C-mol M _V ⁻¹ .d ⁻¹	4	3.69
γ_{light}	mol CH ₂ O.(μmol photons.m ⁻² .s ⁻¹) ⁻¹ .C-mol M _V ⁻¹ .d ⁻¹	0.05	0.0595
ρ_{CO_2,CH_2O}	-	0.9	0.712
γ_{CO_2}	mol CH ₂ O.(μM CO ₂) ⁻¹ .C-mol M _V ⁻¹ .d ⁻¹	1	1.90
$\gamma_{HCO_3^-}$	mol CH ₂ O.(μM HCO ₃ ⁻) ⁻¹ .C-mol M _V ⁻¹ .d ⁻¹	0.02	0.0155
\dot{k}_{CH_2O}	d ⁻¹	2	2.37
$j_{CH_2O,M}$	mol CH ₂ O.C-mol M _V ⁻¹ .d ⁻¹	0.05	0.00
$y_{CH_2O,V}$	mol CH ₂ O.C-mol M _V ⁻¹	1.2	1.00
κ_{CH_2O}	-	0.9	-
j_{m,NO_3^-}	mol NO ₃ ⁻ .C-mol M _V ⁻¹ .d ⁻¹	50	-
$C_{1/2,NO_3^-}$	μM	1	-
$\dot{k}_{NO_3^-}$	d ⁻¹	20	-
$j_{NO_3^-,M}$	mol NO ₃ ⁻ .C-mol M _V ⁻¹ .d ⁻¹	0.05	-
$y_{NO_3^-,V}$	mol NO ₃ ⁻ .C-mol M _V ⁻¹	1.2	-
$\kappa_{NO_3^-}$	-	0.9	-

Table 1: Estimated parameter values for model I, light vs. carbon synthesis. This table shows both the initial estimates used to start up the simplex algorithm, and the final estimates as produced by the simplex algorithm.

Model behavior

Both the curves for growth rate and calcification show a similar, hyperbole-like relationship with respect to the light intensity. However, one subtle but important difference exists: calcification can function at any non-zero light intensity (as it correlates with the light intensity through photosynthesis), whereas population growth requires a certain amount of light to start with. This requirement is caused by maintenance (i.e. $j_{CH_2O,M}$), which consumes some photosynthetically produced CH₂O, and reduces the amount available for growth. Growth can therefore only occur when photosynthesis delivers over $j_{CH_2O,M}$ in CH₂O.

At very low light intensities, the population cannot satisfy its maintenance requirement. At that point, it is proclaimed dead. Thus, the model curves start at the light intensity at which $j_{CH_2O,A} = j_{CH_2O,M}$, $\dot{r} = 0$, and calcification is positive. This also implies that the IC-to-OC ratio has a positive vertical asymptote at precisely that light intensity. This asymptote is not visible in figure 4, due only to the minimal final estimate for $j_{CH_2O,M}$.

As the light intensity increases, both calcification and population growth saturate. The main cause for this is that photosynthesis – on which both processes strongly depend – approaches its maximum rate j_{m,CH_2O} . In addition, the growth rate is intrinsically restricted: part of the CH₂O delivered by $j_{CH_2O,A}$ will never become available for growth, as it is used to ‘fills up’ newly synthesized structural mass. Consequently, increased synthesis of structural mass (i.e. a higher growth rate) decreases the

availability of CH₂O at the growth SU. This is well seen in the kinetics for the catabolic flux $j_{\text{CH}_2\text{O},C} = m_{\text{CH}_2\text{O}} \cdot (\dot{k}_{\text{CH}_2\text{O}} - \dot{r})$: reserve outflow directed at maintenance and growth is hampered by a high growth rate. Note that these mechanisms also imply that the maximum population growth rate does not equal $j_{m,\text{CH}_2\text{O}} / y_{\text{CH}_2\text{O},V}$.

The increases in calcification and growth each are directly affected by $j_{\text{CH}_2\text{O},A}$, but whereas the growth rate is in addition intrinsically restricted, calcification suffers because it is measured per organic carbon present. As the rate of photosynthesis increases, the CH₂O reserve density will too; consequently, calcification per OC will grow relatively slower than photosynthesis.

It is interesting to note that the ratio between calcification and the growth rate appears constant. However, this is due mainly to the extremely low final estimates for $j_{\text{CH}_2\text{O},M}$ and $y_{\text{CH}_2\text{O},V}$. More realistic values of respectively 0.05 and 1.2 would emphasize the vertical asymptote at the lowest viable value of $\{J_{\text{light}}\}$, and cause the ratio to re-increase at higher light intensities.

Quality of fit

Clearly, the model describes the population growth rate very well. The same cannot be said for the description of calcification. The data show it to occur only at higher light intensities ($> 6 \mu\text{mol photons.m}^{-2}.\text{s}^{-1}$), whereas the model dictates that calcification takes place at any positive intensity. Yet the deviations are only slight. Therefore, the description of calcification too might be deemed adequate for most purposes.

However, when both statistics are used to calculate the IC-to-OC ratio, the model fails miserably at delivering an adequate description. Whereas the data clearly show the ratio to equal zero at low light, and to rise with increasing light intensity, the model maintains a constant carbon ratio (even ignoring the theoretical vertical asymptote close to $\{J_{\text{light}}\} = 0$). This is unfortunate, as the IC : OC ratio is a far more important statistic than carbon synthesis rates. The latter are usable in a narrow range of research only, as they require close monitoring of live *Emiliana* specimen. This is not the case for the carbon ratio, which can be determined more or less instantaneously from any sample, living or dead. Hence, more weight should be attributed to the model's description of this ratio, than to those of synthesis rates. Clearly these results give cause for adjustment of the model.

Improving the model

What to change?

Clearly, the model's main defect lies in its description of calcification. In the current model setup, CaCO₃ production is inextricably linked to photosynthesis: the latter obtains part of its CO₂ from calcification under all circumstances. Photosynthesis occurs at any positive light intensity, and hence, calcification does too. This does not match the relationship described by the data: at low light intensity, calcification is absent.

It is not surprising that the model deviates from reality in its description of the calcification-photosynthesis link, as the key kinetics was chosen for simplicity rather than realism. Therefore, the obvious way to enhance the model is to incorporate a realistic representation of the mechanisms surrounding photosynthesis and calcification. Instead of the direct link between the various CO₂ sources and photosynthesis, I chose to include an additional state variable for internal CO₂. Through this variable, sinks and sources interact. To maintain consistency with other parts of the model, the state variable was chosen m_{CO_2} : the amount of CO₂ per C-mole structural mass. Thus, it is comparable with the reserves for CH₂O and NO₃⁻. The differential equation for m_{CO_2} is given by:

$$\frac{d}{dt}m_{\text{CO}_2} = j_{\text{CO}_2,\text{dif}} + j_{\text{CO}_2,\text{calc}} + j_{\text{CO}_2,\text{resp}} - j_{\text{CO}_2,\text{ps}}$$

Here we find the various CO₂ sinks and sources described previously: diffusion, calcification, respiration and photosynthesis.

CO₂ sinks and sources

Since we now have a measure of internal CO₂, diffusion can be described by standard kinetics, i.e. as a function of the external and internal concentration. To obtain the internal concentration, we introduce $[M_V]$, a constant specifying the amount of structural OC per cell volume. The product of $[M_V]$ and m_{CO_2} equals the internal CO₂ concentration. Inward-directed CO₂ diffusion now corresponds to:

$$j_{\text{CO}_2,\text{dif}} = \dot{k}_{d,\text{CO}_2} \cdot (C_{\text{CO}_2} - [M_V] \cdot m_{\text{CO}_2})$$

Here \dot{k}_{d,CO_2} represents the newly introduced diffusion constant. Note that diffusion is taken proportional to structural mass (as $j_{\text{CO}_2,\text{dif}}$ is structural-mass-specific, and independent of M_V), rather than surface area. This is done for simplicity; calculating the true population surface area would require additional parameters and introduce more interdependencies. Diffusion is taken to be proportional to the external CO₂ concentration, which requires rapid diffusion to and from the water layer surrounding the cell. It has been shown, however, that a stagnant, diffusion-limiting water mantle around cells as small as those of *Emiliana huxleyi* is almost non-existent, and of no effect on CO₂ and HCO₃⁻ uptake (Wolf-Gladrow and Riebesell, 1997).

The strongest modification of the model relates to the kinetics for calcification. These are created from scratch, derived from (bio)chemical and physical mechanisms. As described previously, for every CaCO₃ produced in calcification, one molecule of CO₂ is generated. To maintain the high pH required for calcification inside the coccolith vesicle, all produced CO₂ must be exported into the cytoplasm. Clearly, this process would be hindered by a high cytoplasmic CO₂ concentration; as the molecule traverses lipid membranes with relative ease, no means of transport would be able to keep CO₂ out of the vesicle if the cytoplasmic concentration is high enough. It is much more likely that the presence of CO₂ is the controlling factor for calcification, rather than the availability of HCO₃⁻ (which was the main factor of influence in the previous model); the latter substrate is amply available both

inside and outside of the cell. Considering these mechanisms, calcification is well implemented as a process that is restricted only by a M_V -specific maximum rate $j_{m,calc}$, and by a high internal CO₂ pool. For the sake of simplicity, linear kinetics were applied:

$$j_{CO_2,calc} = j_{m,calc} \cdot \left(1 - \frac{m_{CO_2}}{m_{CO_2,no\,calc}} \right)$$

Here $m_{CO_2,no\,calc}$ represents the internal CO₂ density at which no calcification occurs. Note that this form of CO₂ production is mathematically identical to CO₂ diffusion, with respect to m_{CO_2} . Implemented like this, calcification can therefore be regarded a diffusion-enhancer.

Adding respiration-produced CO₂ to the internal pool is straightforward:

$$j_{CO_2,resp} = -(j_{CO_2,M} + j_{CO_2,G})$$

The rate of which CO₂ is consumed by photosynthesis equals $j_{CH_2O,A}$, as every CH₂O produced in photosynthesis requires one CO₂:

$$j_{CO_2,ps} = j_{CH_2O,A}$$

Note that, when m_{CO_2} is regarded a DEB framework-based reserve, this corresponds to complete reincorporation of rejected CO₂ reserves into the pool: the κ_{CO_2} is 1.

CO₂ availability in photosynthesis

As in the original model, the rate of photosynthesis is determined by the availability of its substrates: light and CO₂. However, the availability of the latter substrate is now not determined by its sources directly. Rather, it follows from the size of the internal CO₂ pool. This requires adjustment of j_{CO_2,CH_2O} , the rate at which CO₂ arrives at the photosynthesizing unit. As m_{CO_2} is in all respects similar to a DEB framework-based reserve, it is most logical to describe CO₂ availability with catabolic flux-kinetics, i.e.:

$$j_{CO_2,CH_2O} = m_{CO_2} \cdot (\dot{k}_{CO_2} - \dot{r})$$

For the CO₂ reserve, simplification of the catabolic flux is possible, however. The CO₂ pool differs from the two other reserves in one important aspect: its size. Both the carbohydrate- and nitrate reserve may store large quantities of their respective compounds, sufficient to even duplicate the population in absence of nutrients (i.e. $m_{CH_2O} = y_{CH_2O,V}$, $m_{NO_3^-} = y_{NO_3^-,V}$). The internal CO₂ concentration on the other hand will never far exceed that of the environment, which is at most 25 μM. Assuming $[M_V] = 18$ C-mol.l⁻¹ (Riegman et al., 1998), this corresponds to an m_{CO_2} of approximately $1,4 \cdot 10^{-6}$ mol·C-mol V⁻¹: close to a factor 1,000,000 smaller than the other reserve densities. Still, this small reserve should deliver at least 2 mol CO₂ per C-mol structure per day to photosynthesis if the maximum photosynthetic rate observed in experiments is to be attained. This corresponds to a minimum value for \dot{k}_{CO_2} of 1,440,000 d⁻¹. Clearly, this implies the effect of growth rate \dot{r} – which never exceeds 2 d⁻¹ – on j_{CO_2,CH_2O} is negligible. Therefore, it can be omitted from the equation, resulting in:

$$j_{CO_2,CH_2O} = m_{CO_2} \cdot \dot{k}_{CO_2}$$

The main advantage of this omission is that $\rho_{\text{CO}_2, \text{CH}_2\text{O}}$ (see page 21) now can be assimilated into \dot{k}_{CO_2} , as both constants appear together throughout the model. Thus, the number of parameters is reduced by 1. The rate of photosynthesis is now given by:

$$j_{\text{CH}_2\text{O}, A} = \frac{1}{j_{m, \text{CH}_2\text{O}}^{-1} + (\gamma_{\text{light}} \cdot \{J_{\text{light}}\})^{-1} + (m_{\text{CO}_2} \cdot \dot{k}_{\text{CO}_2})^{-1} - (\gamma_{\text{light}} \cdot \{J_{\text{light}}\} + m_{\text{CO}_2} \cdot \dot{k}_{\text{CO}_2})^{-1}}$$

Net inorganic carbon uptake

The inclusion of the CO₂ pool and its associated kinetics allows for very straightforward descriptions for CO₂- and HCO₃⁻ uptake. CO₂ uptake is merely inward directed diffusion, i.e.:

$$j_{\text{CO}_2 \text{ uptake}} = j_{\text{CO}_2, \text{dif}}$$

HCO₃⁻ uptake follows from the rate of calcification; for every CO₂ produced in CaCO₃ formation, 2 HCO₃⁻ is taken up:

$$j_{\text{HCO}_3^- \text{ uptake}} = 2 \cdot j_{\text{CO}_2, \text{calc}}$$

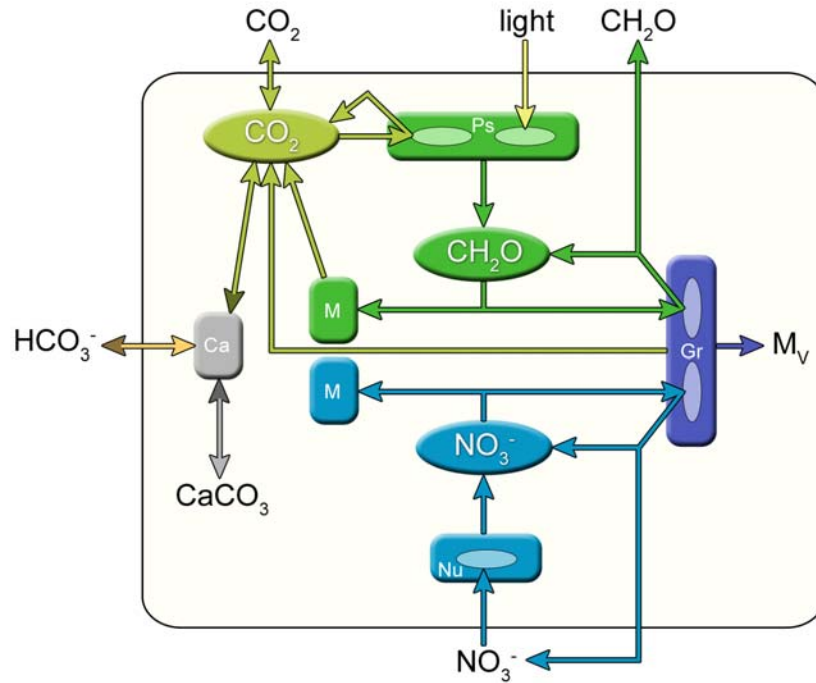


Figure 5: The modeled cell revisited. This figure shows all modeled substance fluxes (arrows), substance transformations (rounded rectangles) and the three reserves (ellipses). Transformations that use synthesizing unit kinetics can be identified by ellipses contained within the rectangle. These ellipses signify required substrate types.

Colors are used to identify pathways of the various compounds: CO₂ (■), light (■), CH₂O (■), HCO₃⁻ (■), CaCO₃ (■), NO₃⁻ (■) and structural mass (■).

The following transformations can be seen: calcification (Ca), photosynthesis (Ps), nitrate uptake (Nu), CH₂O and NO₃⁻ maintenance (M) and synthesis of structural mass (i.e. population growth, Gr). Note that calcification can in principle operate in two directions: standard CaCO₃ production is shown with standard arrowheads, whereas CaCO₃ dissolution is shown with dimmed arrowheads.

For clarity, rejected substrate fluxes that disappear from the scope of the model are not shown. Here, this is the case for light (rejected at the photosynthesizing unit).

Implications for steady state analysis

To describe the behavior of a population in steady state, the kinetics of calcification needed to be modified. Its current linear relationship with m_{CO_2} allows for both positive and negative calcification rates. The latter would imply dissolution of previously produced coccoliths. While such behavior has indeed been described (Sekino et al., 1996; Sekino & Shiraiwa, 1994), it is most definitely not wanted for populations in steady state. If such a population showed negative calcification rates, it would dissolve CaCO₃ ad infinitum. In reality, such behavior would cause rapid destruction of all attached coccoliths, after which $j_{\text{CO}_2, \text{calc}}$ would become 0. Only then would the population truly enter steady state. Hence, calcification in steady state cannot be negative. To ensure $j_{\text{CO}_2, \text{calc}} \geq 0$, a maximum operator is added:

$$j_{\text{CO}_2, \text{calc}} = \max \left(0, j_{m, \text{calc}} \cdot \left(1 - \frac{m_{\text{CO}_2}}{m_{\text{CO}_2, \text{no calc}}} \right) \right)$$

The revised model was analyzed following the same approach as with the original. Steady state analysis was slightly more complicated, as the requirements for steady state are extended by the fact that dm_{CO_2}/dt should equal 0. Thus, the original 1 unknown/1 condition problem (pp. 26 and further) becomes one of 2 unknowns/2 conditions for the revised model: solving steady state requires finding values for \dot{r} and m_{CO_2} that result in (1) the implicit description of \dot{r} to be valid and (2) dm_{CO_2}/dt to equal 0. To this end, the Newton algorithm employed previously was used.

Initial estimates were set to $\dot{r} = 0$ and $m_{\text{CO}_2} = C_{\text{CO}_2}/[M_V]$. Note that the latter setting implies the internal CO₂ concentration is identical to that of the environment (since $C_{\text{CO}_2, \text{int}} = [M_V] \cdot m_{\text{CO}_2}$). Using these initial estimates, realistic steady state values for \dot{r} and m_{CO_2} were found for every set of parameters expected to allow for population survival (obviously no steady state was found when nutrient uptake rates were low and maintenance requirements high, for instance). No additional testing was done to ensure uniqueness of the steady states found.

Results and discussion: model II

Comparison with data

Like the original model, the revised one was fitted to the light-carbon production data (van Bleijswijk, 1996). Incorporation of the CO₂ pool in the model introduced five new parameters related to photosynthesis-calcification interaction (\dot{k}_{d,CO_2} , $[M_V]$, $j_{m,calc}$, $m_{CO_2,no\,calc}$, \dot{k}_{CO_2}), and eliminated three (ρ_{CO_2,CH_2O} , γ_{CO_2} , $\gamma_{HCO_3^-}$). Thus, the number of parameters estimated increases from 8 to 10.

Results are presented in figures 6 to 8. Estimated values for the parameters are included in table 2. As in the original model, the parameters are ill constrained by the data. This can easily be seen by comparing these and previous Simplex estimates for parameters shared across both models: differences in value of a factor 2 are common.

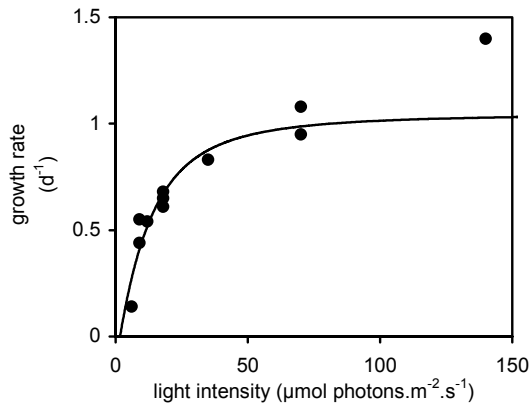


Figure 6: population growth as a function of light intensity.

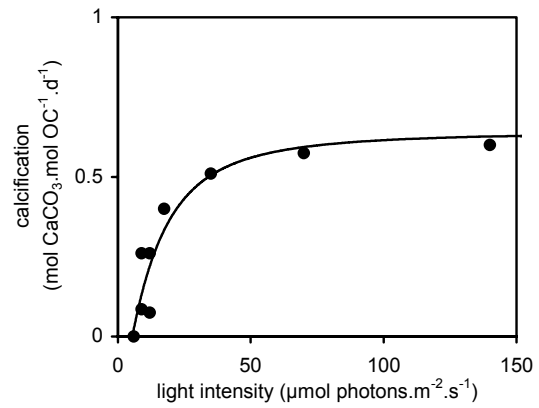


Figure 7: calcification as a function of light intensity.

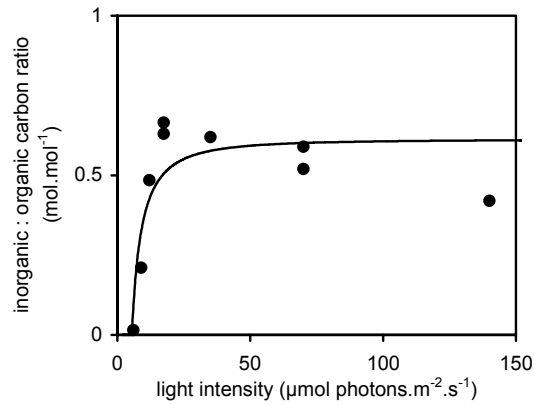


Figure 8: the inorganic carbon : organic carbon ratio as a function of light intensity. This statistic is calculated by dividing the rate of calcification by the rate of organic carbon production (both for the data and the model).

parameter	unit	initial estimate	final estimate
\dot{k}_{d,CO_2}	mol CO ₂ ·(mol CO ₂ ·l ⁻¹) ⁻¹ ·C-mol M _V ⁻¹ ·d ⁻¹	8·10 ⁵	1.39·10 ⁵
[M _V]	C-mol M _V ·l ⁻¹	18	28.6
$j_{m,calc}$	mol CO ₂ ·C-mol M _V ⁻¹ ·d ⁻¹	5	4.83
$m_{CO_2,no\,calc}$	mol CO ₂ ·C-mol M _V ⁻¹	7.5·10 ⁻⁷	4.55·10 ⁻⁷
\dot{k}_{CO_2}	d ⁻¹	10 ⁷	7.85·10 ⁶
j_{m,CH_2O}	mol CH ₂ O·C-mol M _V ⁻¹ ·d ⁻¹	4	5.79
γ_{light}	mol CH ₂ O·(μmol photons·m ⁻² ·s ⁻¹) ⁻¹ ·C-mol M _V ⁻¹ ·d ⁻¹	0.05	0.0825
\dot{k}_{CH_2O}	d ⁻¹	4	2.82
$j_{CH_2O,M}$	mol CH ₂ O·C-mol M _V ⁻¹ ·d ⁻¹	0.05	0.136
$y_{CH_2O,V}$	mol CH ₂ O·C-mol M _V ⁻¹	1.2	1.00
K_{CH_2O}	-	0.9	-
j_{m,NO_3^-}	mol NO ₃ ⁻ ·C-mol M _V ⁻¹ ·d ⁻¹	50	-
$C_{1/2,NO_3^-}$	μmol·l ⁻¹	1	-
$\dot{k}_{NO_3^-}$	d ⁻¹	20	-
$j_{NO_3^-,M}$	mol NO ₃ ⁻ ·C-mol M _V ⁻¹ ·d ⁻¹	0.05	-
$y_{NO_3^-,V}$	mol NO ₃ ⁻ ·C-mol M _V ⁻¹	1.2	-
$K_{NO_3^-}$	-	0.9	-

Table 2: Estimated parameter values for model II, light vs. carbon synthesis. This table shows both the initial estimates used to start up the simplex algorithm, and the final estimates as produced by the simplex algorithm.

Model behavior

Changes in the models behavior occur at 2 points: the rate of calcification, and the rate of photosynthesis.

Through the inclusion of the CO₂ pool, calcification has become more independent of photosynthesis. As photosynthesis consumes internal CO₂, both diffusion and calcification respond through similar, linear kinetics to the drop in m_{CO_2} . However, the parameters specifying their exact response differ. This can well be seen in figure 9, which shows the size of m_{CO_2} , and the contribution of the various CO₂ sources in steady state, using the current parameter estimates. Calcification requires a lower internal CO₂ concentration to function than diffusion, and will therefore begin to function at higher photosynthetic rates, and, consequently, higher light intensities. This mechanism is responsible for the much improved fit of the light intensity-calcification dataset.

The rate of photosynthesis will increase somewhat slower at increasing light intensity, due to changes in CO₂ availability. In the original model, CO₂ availability increased at higher light intensities

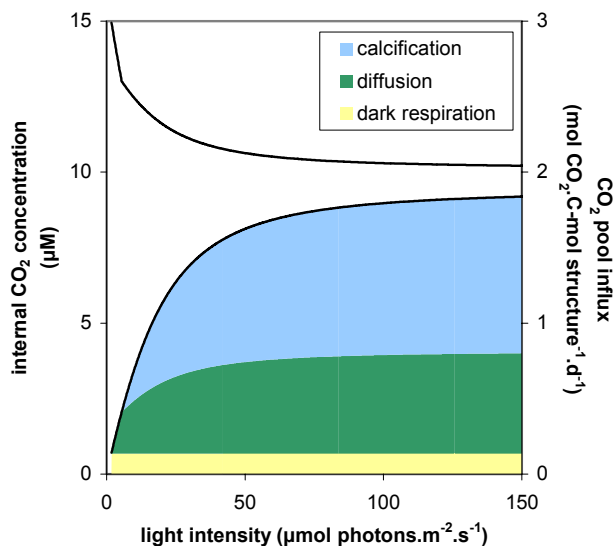


Figure 9: internal CO₂ and various CO₂ sources as a function of light intensity. The internal CO₂ concentration is shown by the black line, while the CO₂ contribution of the various CO₂ sources is shown by the colored surfaces. Note that the total CO₂ influx equals the rate of CO₂ consumption by photosynthesis, as the population is in steady state.

One can clearly see the point at which calcification sets in (around 7 $\mu\text{mol photons.m}^{-2}.\text{s}^{-1}$). Here the initial sharp drop in internal CO₂ ‘softens’. Note that the increased growth rate at high light intensities seems to have no effect on CO₂ arrival from respiration. This is due to the extremely low estimate for the CH₂O-per-V yield.

due to increased growth (which accounts for part of $j_{\text{CO}_2,G}$). In the revised model, however, CO₂ availability drops, which is clearly visible in figure 9.

Discussion

Without a doubt, the revised model does a better job at describing the data. Changes to the rates of organic- and inorganic carbon production are slight, but sufficient to tremendously improve the description of the IC-to-OC ratio. The model still fails to describe the slight decrease in the IC-to-OC ratio at high light intensity shown by the data, but as such behavior is not confirmed by other experiments (Paasche, 1999), it does not hurt application of the model.

Model test case: effects of a global CO₂ increase

While building rather than application of an *Emiliana* model has been the focus of this project, we do present an example of its use. This demonstrates the model's applicability in major areas of research. Fairly recently (September 2000), Riebesell et al. published results of an experiment demonstrating the effects of an oceanic CO₂ increase on the production of OC and CaCO₃ in coccolithophorids. These results give some indication of the potential effects of the global CO₂ increase. Specifically, they can be used to predict whether coccolithophorids will produce a positive or negative feedback. *Emiliana huxleyi* was one of two species studied. The experiments used diluted batch cultures (similar to those performed by van Bleijswijk), which were kept at 5 different concentrations of CO₂.

Methods

The model was simultaneously fitted to two datasets, describing the rates of organic and inorganic carbon synthesis per cell. I assume the number of cells in the population (N) to be proportional to the population's structural mass: $M_V = N \cdot 5 \cdot 10^{-13}$ (Riegman et al., 1998). The conversion factor was derived from the carbon content of light-starved cells, which are unlikely to contain any non-structural carbon¹. Using this relationship, cell-specific synthesis rates were transformed into structural-mass-specific rates. As a result, the datasets can be described as follows:

- Structural-mass-specific organic carbon production equals the production rates of structural carbon and CH₂O reserves combined. Per mole of structure synthesized, an additional $m_{\text{CH}_2\text{O}}$ mole of CH₂O is created in steady state. This results in:

$$\frac{\text{OC synthesis}}{\text{structural mass}} = \dot{r} \cdot (1 + m_{\text{CH}_2\text{O}})$$

- Structural-mass-specific CaCO₃ production equals the rate at which CO₂ is produced in calcification:

$$\frac{\text{CaCO}_3 \text{ synthesis}}{\text{structural mass}} = j_{\text{CO}_2, \text{calc}}$$

In addition, the rates of carbon production were used to calculate the IC : OC ratio. This ratio again applies both to cell contents and net carbon synthesis because the populations are in steady state.

Estimated parameters and their initial estimates were identical to those used for the light-limitation datasets (table 3). Input variables were set to $C_{\text{NO}_3^-} = 6.25 \mu\text{M}$ and $\{J_{\text{light}}\} = 150 \mu\text{mol photons.m}^{-2}.\text{s}^{-1}$ (Riebesell et al., 2000).

Results

Results are presented in figures 10 to 12. Unfortunately, steady state estimation failed at high external CO₂ concentrations (the maximum number of iterations of the Newton routine was exceeded).

The final parameter estimates are included in table 3. Even more than previous datasets, however, these fail to restrain parameter values. The final estimates are completely dependent on the initial estimates chosen, and the values shown in table 1 are provided only to allow for complete result reproduction.

¹ This is of course a rather crude estimate of the conversion factor, as it is derived from other experiments than those delivering the data. Unfortunately, no better measures of structural carbon per cell were available.

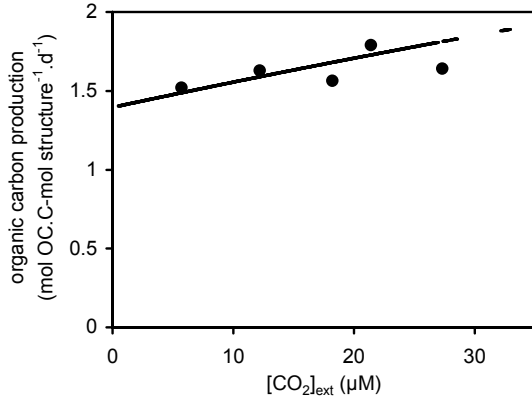


Figure 10: organic carbon production as a function of ambient CO₂. Note that steady state estimation failed at high ambient CO₂.

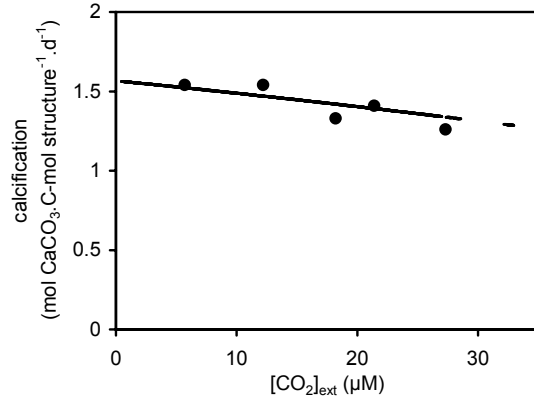


Figure 11: calcification as a function of ambient CO₂. As in figure 10, steady state estimation failed at high ambient CO₂.

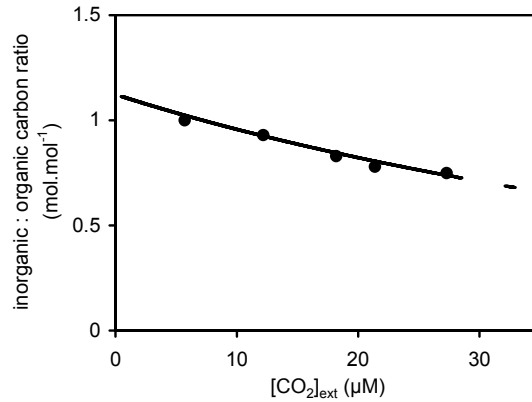


Figure 12: the inorganic carbon : organic carbon ratio as a function of ambient CO₂. This characteristic is calculated by dividing the rates of calcification and organic carbon production.

parameter	unit	initial estimate	final estimate
\dot{k}_{d,CO_2}	mol CO ₂ ·(mol CO ₂ ·l ⁻¹) ⁻¹ ·C-mol M _V ⁻¹ ·d ⁻¹	8·10 ⁵	2.66·10 ⁴
[M _V]	C-mol M _V ·l ⁻¹	18	10.8
$j_{m,calc}$	mol CO ₂ ·C-mol M _V ⁻¹ ·d ⁻¹	5	2.04
$m_{CO_2,no\,calc}$	mol CO ₂ ·C-mol M _V ⁻¹	7.5·10 ⁻⁷	2.54·10 ⁻⁶
\dot{k}_{CO_2}	d ⁻¹	10 ⁷	3.56·10 ⁶
j_{m,CH_2O}	mol CH ₂ O·C-mol M _V ⁻¹ ·d ⁻¹	4	6.77
γ_{light}	mol CH ₂ O·(μmol photons·m ⁻² ·s ⁻¹) ⁻¹ ·C-mol M _V ⁻¹ ·d ⁻¹	0.05	0.0654
\dot{k}_{CH_2O}	d ⁻¹	4	0.0458
$j_{CH_2O,M}$	mol CH ₂ O·C-mol M _V ⁻¹ ·d ⁻¹	0.05	0.0676
$y_{CH_2O,V}$	mol CH ₂ O·C-mol M _V ⁻¹	1.2	2.08
κ_{CH_2O}	-	0.9	-
j_{m,NO_3^-}	mol NO ₃ ⁻ ·C-mol M _V ⁻¹ ·d ⁻¹	50	-
$C_{1/2,NO_3^-}$	μmol·l ⁻¹	1	-
$\dot{k}_{NO_3^-}$	d ⁻¹	20	-
$j_{NO_3^-,M}$	mol NO ₃ ⁻ ·C-mol M _V ⁻¹ ·d ⁻¹	0.05	-
$y_{NO_3^-,V}$	mol NO ₃ ⁻ ·C-mol M _V ⁻¹	1.2	-
$\kappa_{NO_3^-}$	-	0.9	-

Table 3: Estimated parameter values for model II, CO₂ vs. carbon synthesis. This table shows both the initial estimates used to start up the simplex algorithm, and the final estimates as produced by the simplex algorithm.

Discussion

Unfortunately, if there is one thing demonstrated by these fits, it is that the model requires more datasets to reliably predict parameter values. Most estimated values are highly unrealistic, in particular that of \dot{k}_{CH_2O} , which should be about one hundred times as high. The latter deviation is mostly due to the lack of growth data¹: the experiment merely provides data about organic carbon, which can be attributed to either the CH₂O reserve or structure.

An additional problem is that steady state estimation fails at high concentrations of ambient CO₂. This may be due to the highly unrealistic parameter values, but the possibility cannot be excluded that even at realistic values, steady state estimation might fail. This then could only be solved by using better initial estimates for m_{CO_2} and/or \dot{r} .

¹ Though both organic carbon synthesis and inorganic carbon synthesis depend on growth, and should therefore to some extent contain growth data, the datasets are far too limited for this indirect constrain to come out.

General discussion

Clearly, adjustment of the original model is a prerequisite if any broadly applicable *Emiliana* model is to be produced. In its present form, it simply fails to describe one of the most vital statistics used in this line of research. Introduction of a distinctly modeled CO₂ pool eliminates this problem, and renders a model capable of describing the behavior of *Emiliana* in major research scenarios. In addition, it replaces the sole part of the model that used arbitrary, descriptive kinetics, with one based on mechanistic grounds. Therefore, the model is not merely suitable for description of common trends, but can also provide insight in underlying mechanisms.

This in particular applies to the biochemical/physical machinery of calcification, for which numerous hypotheses have been formulated, but rarely tested. My results suggest that very simple physio-chemical interactions involving the internal CO₂ concentration and pH can account for most typical calcification trends. These especially include the correlation between calcification and photosynthesis. The model may also well be able to explain related phenomena, like deviating rates of calcite formation at night (van Bleijswijk, 1996), and the possible functioning of attached coccoliths as a CO₂ source (Sekino et al., 1996). In addition, differences between strains regarding their calcification rate (e.g. the existence of ‘naked’, non-calcifying types) can easily be attributed to slight differences in the parameters for calcification and diffusion. All this would be possible without exhaustively documenting all (bio)chemical pathways involved.

As with any realism-increasing model adjustment, introduction of the CO₂ pool comes with the cost of increased complexity. The number of state variables increases from two to three (although the nitrate pool was ignored for our purposes), and two parameters are added to the already substantial collection. Even more than in the original model, CO₂ influences are felt at every step in the substances pathways: from the initial entry through the cell membrane, to the final creation of new cells. The ensuing interdependencies strongly complicate model analysis. This is clearly visible when the model is fitted to data: slightly ill-chosen initial parameter estimates cause disastrous fits, and a global minimum in the sum-of-squares function – providing one exists at all – is impossible to find. In part, this is of course due to the extremely limited datasets used. One can hardly expect the behavior of two, partly interdependent variables as population growth and calcification to constrain the values of eleven parameters. It might well be possible to produce sound estimates from a well-chosen set of, say, four statistics of the population and individual cells.

However, simplification of model kinetics could significantly facilitate the use of the model. In particular, one can think of removal of the CO₂ pool state variable. Model integration has shown that this pool reaches equilibrium extremely fast compared to both other reserves: this is a matter of milliseconds rather than days (results not published). Thus, for practically every conceivable experiment, the internal CO₂ concentration is well approximated by that in steady state. If we make certain assumptions (e.g. neglecting CO₂ contributions from maintenance and growth), it may well be possible to derive an explicit description of the steady state concentration. This description could replace the true concentration throughout the model, and make analysis much simpler. Such a move is essential if model integration desired, as this currently requires time steps of less than 1/10,000 second due to the volatile nature of the CO₂ pool. Also, it would most likely eliminate any problems with steady state estimation, as seen with the CO₂ datasets (page 42).

While limitation of nutrients beside light and CO₂ has been incorporated in the model (in nitrate), this aspect was mostly neglected during this project. Preliminary results suggest, however, that the model describes the effects of such limitation well. This in particular applies to the relationship between nutrient limitation and growth, calcification and the IC : OC ratio.

Concluding, the final model can describe the types of behavior that are most characteristic for *Emiliana* well. The complexity of the model however is likely to significantly restrain its application; only extensive datasets, describing the behavior of a large number of variables, will allow for reliable parameter estimation.

Summary

Coccolithophorids are a group of unicellular marine algae considered to be responsible for the major part of the earth's calcite production. This process plays an important role in the global carbon cycle, and may to a certain extent affect future developments in atmospheric CO₂. Our aim was to model the physiology of one of the most common coccolithophorids: *Emiliana huxleyi*. The model should allow for application in research related to the global climate and carbon cycle. Using the Dynamic Energy Budget modeling approach (Kooijman, 2000), a dynamic model was constructed that described all major carbon fluxes in a population of *E. huxleyi*, as a function of external light intensity, CO₂, HCO₃⁻ and NO₃⁻. Steady state analysis of this initial model revealed some serious model shortcomings related to the interaction between calcification and photosynthesis. The model was modified to include a biochemically more realistic representation of these processes: an internal CO₂ pool was added, which supplied CO₂ to photosynthesis, and obtained CO₂ from calcification. This corresponds more closely to the current hypotheses regarding calcification. Steady state analysis showed obvious improvements in the behavior of the model. Subsequently, the model was used to describe the behavior of *Emiliana* at various concentrations of ambient CO₂, illustrating the model's use in its targeted area of research. Although the model was able to describe the data, we must conclude that the datasets were too limited to constrain the parameter values. Clearly, the complexity of the model places severe requirements on the quality and quantity of the data used. If these requirements were satisfied, the model could be valuable not only in research related to the global climate, but also to that focusing on the biochemistry and physiology of calcification.

Literature

- Anning, T., Nimer, N., Merrett, M.J., Brownlee, C., 1996. Costs and benefits of calcification in coccolithophorids. *J. Mar. Syst.* 9: 45-56.
- van Bleijswijk, J.D.L., 1996. Ecophysiology of the calcifying marine alga *Emiliana huxleyi*. Thesis, University of Groningen, The Netherlands.
- Brownlee, C., Nimer, N., Dong, L.F., Merrett, M.J., 1994. Cellular regulation during calcification in *Emiliana huxleyi*. In: Green, J.C., Leadbeater, B.S.C. (eds.) *The haptophyte algae*. Clarendon Press, Oxford.
- Buitenhuis, E.T., de Baar, H.J.W., Veldhuis, M.J.W., 1999. Photosynthesis and calcification by *Emiliana huxleyi* (Prymnesiophyceae) as a function of inorganic carbon species. *J. Phycol.* 35: 949-959.
- Burden, R.L., Faires, J.D., 1985. Numerical analysis (3rd edition). Prindle, Weber & Schmidt, Boston.
- Falkowski, P.G., 1994. The role of phytoplankton photosynthesis in global biochemical cycles. *Photosynth. Res.* 39: 235-258.
- Harder, W., Dijkhuizen, L., 1983. Physiological responses to nutrient limitation. *Ann. Rev. Microbiol.* 37: 1-23.
- Kooijman, S.A.L.M., 1998. The Synthesizing Unit as model for the stoichiometric fusion and branching of metabolic fluxes. *Biophys. Chem.* 73: 179-188.
- Kooijman, S.A.L.M., 2000. *Dynamic energy and mass budgets in biological systems* (2nd edition). Cambridge University Press, Cambridge.
- Laws E.A., Thompson, P.A., Popp, B.N., Bidigare, R.R., 1998. Sources of inorganic carbon for marine microalgal photosynthesis: a reassessment of $\delta^{13}\text{C}$ data from batch culture studies of *Thalassiosira pseudonana* and *Emiliana huxleyi*. *Limnol. Oceanogr.* 43(1): 136-142.
- Matsuda, Y., Colman, B., 1995. Induction of CO₂ and bicarbonate transport in the green alga *Chlorella ellipsoidea*. *Plant Physiol.* 108: 247-252.
- Muggli, D.L., Harrison, P.J., 1996. Effects of nitrogen source on the physiology and metal nutrition of *Emiliana huxleyi* grown under different iron and light conditions. *Mar. Ecol. Prog. Ser.* 130: 255-267.
- Nimer, N.A., Brownlee, C., Merrett, M.J., 1994. Carbon dioxide availability, intracellular pH and growth rate of the coccolithophore *Emiliana huxleyi*. *Mar. Ecol. Prog. Ser.* 109: 257-262.
- Paasche, E., 1998. Roles of nitrogen and phosphorus in coccolith formation in *Emiliana huxleyi* (Prymnesiophyceae). *Eur. J. Phycol.* 33: 33-42.
- Paasche, E., 1999. Reduced coccolith calcite production under light-limited growth: a comparative study of three clones of *Emiliana huxleyi* (Prymnesiophyceae). *Phycologia* 38(6): 508-516.
- Riebesell, U., Zondervan, I., Rost, B., Tortell, P.D., Zeebe, R.E., Morel, F.M.M., 2000. Reduced calcification of marine plankton in response to increased atmospheric CO₂. *Nature* 407: 364-367.
- Riegman, R., Stolte, W., Noordeloos, A.A.M., 1998. A model system approach to biological climate forcing: the example of *Emiliana huxleyi*. Subproject (b): Physiology. Final report, Netherlands Institute for Sea Research.

- Sekino, K., Kobayashi, H., Shiraiwa, Y., 1996. Role of coccoliths in the utilization of inorganic carbon by a marine unicellular coccolithophorid, *Emiliana huxleyi*: a survey using intact cells and protoplasts. *Plant Cell Physiol.* 37(2): 123-127.
- Sekino, K., Shiraiwa, Y., 1994. Accumulation and utilization of dissolved inorganic carbon by a marine unicellular coccolithophorid, *Emiliana huxleyi*. *Plant Cell Physiol.* 35(3): 353-361.
- Thompson, P.A., Calvert, S.E., 1995. Carbon isotope fractionation by *Emiliana huxleyi*. *Limnol. Oceanogr.* 40(4): 673-679.
- Wolf-Gladrow, D., Riebesell, U., 1997. Diffusion and reactions in the vicinity of plankton: a refined model for inorganic carbon transport. *Mar. Chem.* 59: 17-34.
- Zonneveld, C., 1996. Modelling the kinetics of non-limiting nutrients in microalgae. *J. Mar. Syst.* 9: 121-136.
- Zonneveld, C., 1998. Light-limited microalgal growth: a comparison of modeling approaches. *Ecol. Modell.* 113: 41-54.

Appendix A: Equations and parameters of model I

carbon pathways

$$j_{\text{CH}_2\text{O},A} = \frac{1}{j_{m,\text{CH}_2\text{O}}^{-1} + (\gamma_{\text{light}} \cdot \{J_{\text{light}}\})^{-1} + j'_{\text{CO}_2,\text{CH}_2\text{O}}^{-1} - (\gamma_{\text{light}} \cdot \{J_{\text{light}}\} + j'_{\text{CO}_2,\text{CH}_2\text{O}})^{-1}}$$

$$j'_{\text{CO}_2,\text{CH}_2\text{O}} = \rho_{\text{CO}_2,\text{CH}_2\text{O}} \cdot (\gamma_{\text{CO}_2} \cdot C_{\text{CO}_2} + \gamma_{\text{HCO}_3^-} \cdot C_{\text{HCO}_3^-} + j_{\text{CH}_2\text{O},M} + \dot{r} \cdot (\dot{k}_{\text{CH}_2\text{O},V} - 1))$$

$$\frac{d}{dt} m_{\text{CH}_2\text{O}} = j_{\text{CH}_2\text{O},A} - \dot{k}_{\text{CH}_2\text{O}} \cdot m_{\text{CH}_2\text{O}} + \kappa_{\text{CH}_2\text{O}} \cdot j_{\text{CH}_2\text{O},R}$$

$$j_{\text{CH}_2\text{O},C} = m_{\text{CH}_2\text{O}} \cdot (\dot{k}_{\text{CH}_2\text{O}} - \dot{r})$$

$$j_{\text{CH}_2\text{O},G} = j_{\text{CH}_2\text{O},C} - j_{\text{CH}_2\text{O},M}$$

$$j_{\text{CH}_2\text{O},R} = j_{\text{CH}_2\text{O},G} - y_{\text{CH}_2\text{O},V} \cdot \dot{r}$$

nitrate pathways

$$j_{\text{NO}_3^-,A} = j_{m,\text{NO}_3^-} \cdot \frac{C_{\text{NO}_3^-}}{C_{\text{NO}_3^-} + C_{\frac{1}{2},\text{NO}_3^-}}$$

$$\frac{d}{dt} m_{\text{NO}_3^-} = j_{\text{NO}_3^-,A} - \dot{k}_{\text{NO}_3^-} \cdot m_{\text{NO}_3^-} + \kappa_{\text{NO}_3^-} \cdot j_{\text{NO}_3^-,R}$$

$$j_{\text{NO}_3^-,C} = m_{\text{NO}_3^-} \cdot (\dot{k}_{\text{NO}_3^-} - \dot{r})$$

$$j_{\text{NO}_3^-,G} = j_{\text{NO}_3^-,C} - j_{\text{NO}_3^-,M}$$

$$j_{\text{NO}_3^-,R} = j_{\text{NO}_3^-,G} - y_{\text{NO}_3^-,V} \cdot \dot{r}$$

population growth (synthesis of structural mass)

$$\dot{r} = \frac{1}{\left(\frac{j_{\text{CH}_2\text{O},G}}{y_{\text{CH}_2\text{O},V}}\right)^{-1} + \left(\frac{j_{\text{NO}_3^-,G}}{y_{\text{NO}_3^-,V}}\right)^{-1} - \left(\frac{j_{\text{CH}_2\text{O},G}}{y_{\text{CH}_2\text{O},V}} + \frac{j_{\text{NO}_3^-,G}}{y_{\text{NO}_3^-,V}}\right)^{-1}}$$

parameter	dimension	interpretation
j_{m,CH_2O}	mol CH ₂ O.C-mol M _V ⁻¹ .d ⁻¹	maximum rate of photosynthesis per present structural mass
γ_{light}	mol CH ₂ O.(μmol photons.m ⁻² .s ⁻¹) ⁻¹ .C-mol M _V ⁻¹ .d ⁻¹	potential CH ₂ O yield per light intensity unit per present structural mass
ρ_{CO_2,CH_2O}	-	binding probability of arriving CO ₂ with respect to CH ₂ O SU (= part of dissimilative CO ₂ usable in photosynthesis)
γ_{CO_2}	mol CH ₂ O.(μM CO ₂) ⁻¹ .C-mol M _V ⁻¹ .d ⁻¹	diffusive CO ₂ arrival at CH ₂ O SU per external CO ₂ concentration per present structural mass
$\gamma_{HCO_3^-}$	mol CH ₂ O.(μM HCO ₃ ⁻) ⁻¹ .C-mol M _V ⁻¹ .d ⁻¹	potential CO ₂ production in calcification per external HCO ₃ ⁻ concentration per present structural mass
\dot{k}_{CH_2O}	d ⁻¹	maximum outflow rate of the CH ₂ O reserve density
$j_{CH_2O,M}$	mol CH ₂ O.C-mol M _V ⁻¹ .d ⁻¹	CH ₂ O required for maintenance of structural mass per time
$y_{CH_2O,V}$	mol CH ₂ O.C-mol M _V ⁻¹	CH ₂ O required per synthesized structural mass
κ_{CH_2O}	-	part of rejected CH ₂ O reserve (rejected at growth SU) that returns to the CH ₂ O reserve pool
j_{m,NO_3^-}	mol NO ₃ ⁻ .C-mol M _V ⁻¹ .d ⁻¹	maximum rate of nitrate assimilation per present structural mass
$C_{\frac{1}{2},NO_3^-}$	μM	external nitrate concentration at which nitrate assimilation occurs at half of its maximum rate
$\dot{k}_{NO_3^-}$	d ⁻¹	maximum outflow rate of the NO ₃ ⁻ reserve density
$j_{NO_3^-,M}$	mol NO ₃ ⁻ .C-mol M _V ⁻¹ .d ⁻¹	NO ₃ ⁻ required for maintenance of structural mass per time
$y_{NO_3^-,V}$	mol NO ₃ ⁻ .C-mol M _V ⁻¹	NO ₃ ⁻ required per synthesized structural mass
$\kappa_{NO_3^-}$	-	part of rejected NO ₃ ⁻ reserve (rejected at growth SU) that returns to the NO ₃ ⁻ reserve pool

Appendix B: Equations and parameters of model II

CO₂ pathways

$$\frac{d}{dt}m_{CO_2} = j_{CO_2,dif} + j_{CO_2,calc} + j_{CO_2,resp} - j_{CH_2O,A}$$

$$j_{CO_2,dif} = \dot{k}_{d,CO_2} \cdot (C_{CO_2} - [M_V] \cdot m_{CO_2})$$

$$j_{CO_2,calc} = j_{m,calc} \cdot \left(1 - \frac{m_{CO_2}}{m_{CO_2,no\ calc}}\right)$$

$$j_{CO_2,resp} = j_{CH_2O,M} + \dot{r} \cdot (y_{CH_2O,V} - 1)$$

CH₂O pathways

$$j_{CH_2O,A} = \frac{1}{j_{m,CH_2O}^{-1} + (\gamma_{light} \cdot \{J_{light}\})^{-1} + (m_{CO_2} \cdot \dot{k}_{CO_2})^{-1} - (\gamma_{light} \cdot \{J_{light}\} + m_{CO_2} \cdot \dot{k}_{CO_2})^{-1}}$$

$$\frac{d}{dt}m_{CH_2O} = j_{CH_2O,A} - \dot{k}_{CH_2O} \cdot m_{CH_2O} + \kappa_{CH_2O} \cdot j_{CH_2O,R}$$

$$j_{CH_2O,C} = m_{CH_2O} \cdot (\dot{k}_{CH_2O} - \dot{r})$$

$$j_{CH_2O,G} = j_{CH_2O,C} - j_{CH_2O,M}$$

$$j_{CH_2O,R} = j_{CH_2O,G} - y_{CH_2O,V} \cdot \dot{r}$$

nitrate pathways

$$j_{NO_3^-,A} = j_{m,NO_3^-} \cdot \frac{C_{NO_3^-}}{C_{NO_3^-} + C_{\frac{1}{2},NO_3^-}}$$

$$\frac{d}{dt}m_{NO_3^-} = j_{NO_3^-,A} - \dot{k}_{NO_3^-} \cdot m_{NO_3^-} + \kappa_{NO_3^-} \cdot j_{NO_3^-,R}$$

$$j_{NO_3^-,C} = m_{NO_3^-} \cdot (\dot{k}_{NO_3^-} - \dot{r})$$

$$j_{NO_3^-,G} = j_{NO_3^-,C} - j_{NO_3^-,M}$$

$$j_{NO_3^-,R} = j_{NO_3^-,G} - y_{NO_3^-,V} \cdot \dot{r}$$

population growth (synthesis of structural mass)

$$\dot{r} = \frac{1}{\left(\frac{j_{CH_2O,G}}{y_{CH_2O,V}}\right)^{-1} + \left(\frac{j_{NO_3^-,G}}{y_{NO_3^-,V}}\right)^{-1} - \left(\frac{j_{CH_2O,G}}{y_{CH_2O,V}} + \frac{j_{NO_3^-,G}}{y_{NO_3^-,V}}\right)^{-1}}$$

parameter	dimension	interpretation
\dot{k}_{d,CO_2}	mol CO ₂ .(M CO ₂) ⁻¹ .C-mol M _V ⁻¹ .d ⁻¹	diffusion rate of CO ₂ between environment and cytoplasm, per concentration difference, per structural mass per time
$[M_V]$	C-mol M _V .l ⁻¹	structural mass present per population volume
$j_{m,calc}$	mol CO ₂ .C-mol M _V ⁻¹ .d ⁻¹	maximum rate of calcification (in amount of CO ₂ formed) per structural mass per day
$m_{CO_2,no\ calc}$	mol CO ₂ .C-mol M _V ⁻¹	internal CO ₂ density (amount of CO ₂ per structural mass) at which no net production or dissolution of CaCO ₃ occurs
\dot{k}_{CO_2}	d ⁻¹	outflow rate of the CO ₂ reserve
j_{m,CH_2O}	mol CH ₂ O.C-mol V ⁻¹ .d ⁻¹	maximum rate of photosynthesis per present structural mass
γ_{light}	mol CH ₂ O.(μmol photons.m ⁻² .s ⁻¹) ⁻¹ .C-mol M _V ⁻¹ .d ⁻¹	potential CH ₂ O yield per light intensity unit per present structural mass
\dot{k}_{CH_2O}	d ⁻¹	maximum outflow rate of the CH ₂ O reserve density
$j_{CH_2O,M}$	mol CH ₂ O.C-mol M _V ⁻¹ .d ⁻¹	CH ₂ O required for maintenance of structural mass per time
$Y_{CH_2O,V}$	mol CH ₂ O.C-mol M _V ⁻¹	CH ₂ O required per synthesized structural mass
κ_{CH_2O}	-	part of rejected CH ₂ O reserve (rejected at growth SU) that returns to the CH ₂ O reserve pool
j_{m,NO_3^-}	mol NO ₃ ⁻ .C-mol M _V ⁻¹ .d ⁻¹	maximum rate of nitrate assimilation per present structural mass
$C_{\frac{1}{2},NO_3^-}$	μM	external nitrate concentration at which nitrate assimilation occurs at half of its maximum rate
$\dot{k}_{NO_3^-}$	d ⁻¹	maximum outflow rate of the NO ₃ ⁻ reserve density
$j_{NO_3^-,M}$	mol NO ₃ ⁻ .C-mol M _V ⁻¹ .d ⁻¹	NO ₃ ⁻ required for maintenance of structural mass per time
$Y_{NO_3^-,V}$	mol NO ₃ ⁻ .C-mol M _V ⁻¹	NO ₃ ⁻ required per synthesized structural mass
$\kappa_{NO_3^-}$	-	part of rejected NO ₃ ⁻ reserve (rejected at growth SU) that returns to the NO ₃ ⁻ reserve pool

Appendix C: When to use fluxes instead of concentrations

One of the most remarkable aspects of the SU kinetics is that it deals with substrate arrival fluxes instead of substrate concentrations. Where Michaelis-Menten kinetics specifies $k \cdot X$ (k being a constant and X being substrate concentration), SU kinetics uses $\rho_{X,P} \cdot J_X / y_{X,P}$. Herein $\rho_{X,P}$ is the binding probability of X to the SU producing P , J_X is the arrival flux of X and $y_{X,P}$ is the number of units of X required for one unit of P (yield). While this approach might seem to be conceptually very different from concentration-based kinetics, both are in fact closely related. In fact, in most SU applications flux-based kinetics can be shown to equal true concentration-based kinetics if three conditions are met.

Kooijman's choice to use fluxes instead of concentrations finds its value in my opinion mainly in its implicit simplifications of concentration-based kinetics, rather than in its view on reaction mechanics. Its simplifying properties become clear when describing internal SU transformations. If these transformations were described by concentration-based kinetics, incorporation of additional state variables would be required, because internal substrate concentrations are a part of the state of the cell. Instead, the flux-based approach takes the SU rate to be a function of the substrate input flux. All substrate that was offered to the SU but not immediately transformed into product is rejected and does not influence the transformation rate any further. To make the flux-based approach a valid replacement for the concentration-based approach, the following must be true:

$$k \cdot X_{in} = \frac{\rho_{X,P}}{y_{X,P}} \cdot J_X$$

for $\rho_{X,P} \cdot J_X / y_{X,P}$ is the flux-based replacement of the concentration-based $k \cdot X_{in}$. Since the value of constant $\rho_{X,P}$ cannot be determined independently of SU kinetics, the main requirement for X_{in} is that it is a linear function of J_X .

In a concentration-based approach, every substrate would require its own state variable: internal substrate concentration. The differential for those state variables would look like this:

$$\frac{d}{dt} X_{in} = J_X - y_{X,P} \cdot J_{P,A}(k \cdot X_{in}, \dots) - J_{X,out}(X_{in}, \dots),$$

X_{in}	internal concentration of substrate X
J_X	arrival flux of substrate X (identical to J_X in flux-based kinetics)
$J_{P,A}(k \cdot X_{in}, \dots)$	concentration-based SU function: assimilation flux of product P
$J_{X,out}(X_{in}, \dots)$	substrate flux disappearing from the substrate pool without any involvement in the SU transformation

$J_{X,out}(X_{in}, \dots)$ is added to represent the 'rejected substrate flux' of flux-based SU kinetics, and is – using concentration-based kinetics – assumed to independent of the rate at which substrate arrives. This would be the case when substrate disappears through diffusion, for instance.

As shown above, flux-based kinetics can replace concentration-based kinetics if X_{in} is a linear function of J_X , the substrate currently arriving. Since current substrate arrival rates are independent of previous ones, it requires X_{in} to be independent of earlier arrived substrate too, or:

$$\begin{aligned} \frac{d}{dt} X_{in} &= J_X - y_{X,P} \cdot J_{P,A}(k \cdot X_{in}, \dots) - J_{X,out}(X_{in}, \dots) = 0 \\ J_X &= y_{X,P} \cdot J_{P,A}(k \cdot X_{in}, \dots) + J_{X,out}(X_{in}, \dots) \end{aligned}$$

This is the first condition: to replace concentration-based kinetics, flux-based kinetics requires a constant internal substrate concentration.

Clearly, when we assume SU transformation rate and substrate outflow are independent of substrate inflow, X_{in} can only be linear function of J_X if $y_{X,P} \cdot J_{P,A}(X_{in}, \dots) + J_{X,out}(X_{in}, \dots)$ is a linear function of X_{in} :

$$\begin{aligned} y_{X,P} \cdot J_{P,A}(k \cdot X_{in}, \dots) + J_{X,out}(X_{in}, \dots) &= c \cdot X_{in}, \text{ or} \\ J_{X,out}(X_{in}, \dots) &= c \cdot X_{in} - y_{X,P} \cdot J_{P,A}(k \cdot X_{in}, \dots), \end{aligned}$$

with c being an unknown constant.

We know the SU function $J_{P,A}(k \cdot X_{in}, \dots)$ to show a hyperbole-like response to an increasing X_{in} . For $y_{X,P} \cdot J_{P,A}(k \cdot X_{in}, \dots) + J_{X,out}(X_{in}, \dots)$ to be a linear function of the internal substrate concentration, $J_{X,out}(X_{in}, \dots)$ would have to supplement the SU function in order to arrive at $c \cdot X_{in}$.

This is the second condition: to replace concentration-based kinetics, flux-based kinetics requires the substrate outflow, or ‘rejected flux’ to show a relationship to X_{in} similar to $c \cdot X_{in} - y_{X,P} \cdot J_{P,A}(k \cdot X_{in}, \dots)$.

While the first condition is probably met in most circumstances (i.e. the changes in internal substrate concentration are negligible compared to the turnover rate of internal substrate), the second one is not.

In the simple case of substrate outflow through diffusion, its relationship with X_{in} will be $d \cdot X_{in}$, with d being the diffusion constant. The flux-based approach resulting in an outflow of $c \cdot X_{in} - y \cdot g(X_{in}, \dots)$ will then only be a valid in the following situations:

- The SU transformation rate is negligible compared to the outflow through diffusion. c then is identical to the diffusion constant d .
- X_{in} stays relatively small, thereby making $c_1 \cdot X_{in}$ (c_1 being an unknown constant) an adequate approximation for the SU transformation rate. c then becomes $d - c_1$.

The flux-based approach is better not used in situations where substrate outflow (or rejected substrate flux) is small compared to the SU transformation rate, and the SU runs at speeds close to its maximum. The decision to use the flux-based approach should depend strongly on the destination of rejected substrate, and expected outflow-kinetics. The recommendation given above only applies in situations where substrate outflow is expected to resemble $d \cdot X_{in}$, as with diffusion.